EUROPEAN ORGANISATION FOR NUCLEAR RESEARCH

CERN-EP/90-27
February 23, 1990

A Combined Analysis of the Hadronic and Leptonic Decays of the Z^0

The OPAL Collaboration

M.Z. Akrawy[11], G. Alexander[21], J. Allison[14], P.P. Allport[5], K.J. Anderson[8], J.C. Armitage[6], G.T.J. Arnison[18], P. Ashton[14], G. Azuelos[16,f], J.T.M. Baines[14], A.H. Ball[15], J. Banks[14], G.J. Barker[11], R.J. Barlow[14], J.R. Batley[5], J. Becker[9], T. Behnke[7], K.W. Bell[18], G. Bella[21], S. Bethke[10], O. Biebel[3], U. Binder[9], I.J. Bloodworth[1], P. Bock[10], H. Breuker[7], R.M. Brown[18], R. Brun[7], A. Buijs[7], H.J. Burckhart[7], P. Capiluppi[2], R.K. Carnegie[6], A.A. Carter[11], J.R. Carter[5], C.Y. Chang[15], D.G. Charlton[7], J.T.M. Chrin[14], I. Cohen[21], W.J. Collins[5], J.E. Conboy[13], M. Couch[1], M. Coupland[12], M. Cuffiani[2], S. Dado[20], G.M. Dallavalle[2], M.M. Deninno[2], A. Dieckmann[10], M. Dittmar[4], M.S. Dixit[17], E. Duchovni[24], I.P. Duerdoth[7,d], D. Dumas[6], H. El Mamouni[16], P.A. Elcombe[5], P.G. Estabrooks[6], E. Etzion[21], F. Fabbri[2], P. Farthouat[19], H.M. Fischer[3], D.G. Fong[15], M.T. French[18], C. Fukunaga[22], B. Gandois[19], O. Ganel[24], J.W. Gary[10], J. Gascon[16], N.I. Geddes[18], C.N.P. Gee[18], C. Geich-Gimbel[3], S.W. Gensler[8], F.X. Gentit[19], G. Giacomelli[2], V. Gibson[5], W.R. Gibson[11], J.D. Gillies[18], J. Goldberg[20], M.J. Goodrick[5], W. Gorn[4], D. Granite[20], E. Gross[24], P. Grosse-Wiesmann[7], J. Grunhaus[21], H. Hagedorn[9], J. Hagemann[7], M. Hansroul[7], C.K. Hargrove[17], J. Hart[5], P.M. Hattersley[1], M. Hauschild[7], C.M. Hawkes[7], E. Heflin[4], R.J. Hemingway[6], R.D. Heuer[7], J.C. Hill[5], S.J. Hillier[1], C. Ho[4], J.D. Hobbs[8], P.R. Hobson[23], D. Hochman[24], B. Holl[7], R.J. Homer[1], S.R. Hou[15], C.P. Howarth[13], R.E. Hughes-Jones[14], P. Igo-Kemenes[10], H. Ihssen[10], D.C. Imrie[23], A. Jawahery[15], P.W. Jeffreys[18], H. Jeremie[16], M. Jimack[7], M. Jobes[1], R.W.L. Jones[11], P. Jovanovic[1], D. Karlen[6], K. Kawagoe[22], T. Kawamoto[22], R.G. Kellogg[15], B.W. Kennedy[13], C. Kleinwort[7], D.E. Klem[17], G. Knop[3], T. Kobayashi[22], T.P. Kokott[3], L. Köpke[7], R. Kowalewski[6], H. Kreutzmann[3], J. von Krogh[10], J. Kroll[8], M. Kuwano[22], P. Kyberd[11], G.D. Lafferty[14], F. Lamarche[16], W.J. Larson[4], M.M.B. Lasota[11], J.G. Layter[4], P. Le Du[19], P. Leblanc[16], A.M. Lee[15], D. Lellouch[7], P. Lennert[10], L. Lessard[16], L. Levinson[24], S.L. Lloyd[11], F.K. Loebinger[14], J.M. Lorah[15], B. Lorazo[16], M.J. Losty[17], J. Ludwig[9], N. Lupu[20], J. Ma[4,b], A.A. Macbeth[14], M. Mannelli[7], S. Marcellini[2], G. Maringer[3], A.J. Martin[11], J.P. Martin[16], T. Mashimo[22], P. Mättig[7], U. Maur[3], T.J. McMahon[1], A.C. McPherson[6,c], F. Meijers[7], D. Menszner[10], F.S. Merritt[8], H. Mes[17], A. Michelini[7], R.P. Middleton[18], G. Mikenberg[24], D.J. Miller[13], C. Milstene[21], M. Minowa[22], W. Mohr[9], A. Montanari[2], T. Mori[22], M.W. Moss[14], A. Muller[19], P.G. Murphy[14], W.J. Murray[5], B. Nellen[3], H.H. Nguyen[8], M. Nozaki[22], A.J.P. O'Dowd[14], S.W. O'Neale[7,e], B.P. O'Neill[4], F.G. Oakham[17], F. Odorici[2], M. Ogg[6], H. Oh[4], M.J. Oreglia[8], S. Orito[22], G.N. Patrick[18],

S.J. Pawley[14], P. Pfister[9], J.E. Pilcher[8], J.L. Pinfold[24], D.E. Plane[7], B. Poli[2], A. Pouladdej[6], T.W. Pritchard[11], G. Quast[7], J. Raab[7], M.W. Redmond[8], D.L. Rees[1], M. Regimbald[16], K. Riles[4], C.M. Roach[5], S.A. Robins[11], A. Rollnik[3], J.M. Roney[8], S. Rossberg[9], A.M. Rossi[2,a], P. Routenburg[6], K. Runge[9], O. Runolfsson[7], S. Sanghera[6], R.A. Sansum[18], M. Sasaki[22], B.J. Saunders[18], A.D. Schaile[9], O. Schaile[9], W. Schappert[6], P. Scharff-Hansen[7], H. von der Schmitt[10], S. Schreiber[3], J. Schwarz[9], A. Shapira[24], B.C. Shen[4], P. Sherwood[13], A. Simon[3], G.P. Siroli[2], A. Skuja[15], A.M. Smith[7], T.J. Smith[1], G.A. Snow[15], E.J. Spreadbury[13], R.W. Springer[15], M. Sproston[18], K. Stephens[14], H.E. Stier[9], R. Ströhmer[10], D. Strom[8], H. Takeda[22], T. Takeshita[22], T. Tsukamoto[22], M.F. Turner[5], G. Tysarczyk-Niemeyer[10], D. Van den plas[16], G.J. VanDalen[4], C.J. Virtue[17], A. Wagner[10], C. Wahl[9], C.P. Ward[5], D.R. Ward[5], J. Waterhouse[6], P.M. Watkins[1], A.T. Watson[1], N.K. Watson[1], M. Weber[10], S. Weisz[7], N. Wermes[10], M. Weymann[7], G.W. Wilson[7], J.A. Wilson[1], I. Wingerter[7], V-H. Winterer[9], N.C. Wood[13], S. Wotton[7], B. Wuensch[3], T.R. Wyatt[14], R. Yaari[24], Y. Yang[4,b], G. Yekutieli[24], T. Yoshida[22], W. Zeuner[7], G.T. Zorn[15], S. Zylberajch[19].

[1]School of Physics and Space Research, University of Birmingham, Birmingham, B15 2TT, UK
[2]Dipartimento di Fisica dell' Università di Bologna and INFN, Bologna, 40126, Italy
[3]Physikalisches Institut, Universität Bonn, D-5300 Bonn 1, FRG
[4]Department of Physics, University of California, Riverside, CA 92521 USA
[5]Cavendish Laboratory, Cambridge, CB3 0HE, UK
[6]Carleton University, Dept of Physics, Colonel By Drive, Ottawa, Ontario K1S 5B6, Canada
[7]CERN, European Organisation for Particle Physics, 1211 Geneva 23, Switzerland
[8]Enrico Fermi Institute and Department of Physics, University of Chicago, Chicago Illinois 60637, USA
[9]Fakultät für Physik, Albert Ludwigs Universität, D-7800 Freiburg, FRG
[10]Physikalisches Institut, Universität Heidelberg, D-6900 Heidelberg, FRG
[11]Queen Mary and Westfield College, University of London, London, E1 4NS, UK
[12]Birkbeck College, London, WC1E 7HV, UK
[13]University College London, London, WC1E 6BT, UK
[14]Department of Physics, Schuster Laboratory, The University, Manchester, M13 9PL, UK
[15]Department of Physics and Astronomy, University of Maryland, College Park, Maryland 20742, USA
[16]Laboratoire de Physique Nucléaire, Université de Montréal, Montréal, Quebec, H3C 3J7, Canada
[17]National Research Council of Canada, Herzberg Institute of Astrophysics, Ottawa, Ontario K1A 0R6, Canada
[18]Rutherford Appleton Laboratory, Chilton, Didcot, Oxfordshire, OX11 0QX, UK
[19]DPhPE, CEN Saclay, F-91191 Gif-sur-Yvette, France
[20]Department of Physics, Technion-Israel Institute of Technology, Haifa 32000, Israel
[21]Department of Physics and Astronomy, Tel Aviv University, Tel Aviv 69978, Israel
[22]International Centre for Elementary Particle Physics and Dept of Physics, University of Tokyo, Tokyo 113, and Kobe University, Kobe 657, Japan
[23]Brunel University, Uxbridge, Middlesex, UB8 3PH UK
[24]Nuclear Physics Department, Weizmann Institute of Science, Rehovot, 76100, Israel

[a]Present address: Dipartimento di Fisica, Università della Calabria, 87036 Rende, Italy
[b]On leave from Harbin Institute of Technology, Harbin, China
[c]Now at Applied Silicon Inc
[d]On leave from Manchester University
[e]On leave from Birmingham University
[f]and TRIUMF, Vancouver, Canada

(submitted to Phys. Lett.)

This paper is dedicated to the memory of Elizabeth Spreadbury

who died on February 6th 1990.

Abstract

We report on a measurement of the mass of the Z^0 boson, its total width, and its partial decay widths into hadrons and leptons. On the basis of 25,801 hadronic decays and 1,999 decays into electrons, muons or taus, selected over eleven energy points between 88.28 GeV and 95.04 GeV, we obtain from a combined fit to hadrons and leptons a mass of $M_Z = 91.154 \pm 0.021$ (exp)$\pm$ 0.030 (LEP) GeV, and a total width of $\Gamma_Z = 2.536 \pm 0.045$ GeV. The errors on M_Z have been separated into the experimental error and the uncertainty due to the LEP beam energy. The measured leptonic partial widths are $\Gamma_{ee} = 81.2 \pm 2.6$ MeV, $\Gamma_{\mu\mu} = 82.6 \pm 5.8$ MeV, and $\Gamma_{\tau\tau} = 85.7 \pm 7.1$ MeV, consistent with lepton universality. From a fit assuming lepton universality we obtain $\Gamma_{l^+l^-} = 81.9 \pm 2.0$ MeV. The hadronic partial width is $\Gamma_{had} = 1838 \pm 46$ MeV. From the measured total and partial widths a model independent value for the invisible width is calculated to be $\Gamma_{inv} = 453 \pm 44$ MeV. The errors quoted include both the statistical and the systematic uncertainties.

1 Introduction

The Standard Model, describing the unification of the weak and electromagnetic interactions, contains as a central element the massive vector boson Z^0, the neutral carrier of the weak force. Following the successful start of the new accelerators SLC and LEP several groups presented their first measurements of the parameters of the Z^0 [1]-[5]. Some of these measurements have recently been updated taking into account most of the currently available data [6]. We present here a measurement of the parameters of the Z^0, based on the entire data sample collected in 1989 with the OPAL detector. This corresponds to a sixfold increase in luminosity compared with our previous publications [4,7]. An improved understanding of the detector has led to a significant reduction in the systematic uncertainties of the measurements.

In this publication we present a combined analysis of the hadronic and leptonic decays of the Z^0 based on a measurement of the hadronic and leptonic cross sections as a function of energy. The cross sections were measured at 11 centre-of-mass energies between 88.28 and 95.04 GeV by repeatedly scanning across the Z^0 resonance. Measurements at nearby energies, within 10 MeV, were combined into one data point at the luminosity-weighted average energy. The measurement of the energies was performed by the LEP Division. The residual fractional error in the energy of each beam was $3 \cdot 10^{-4}$, corresponding to 30 MeV in the centre-of-mass energy. This error enters as a scale uncertainty in the measurement of the Z^0 mass. The fractional point-to-point error in the energy was $1 \cdot 10^{-4}$. The centre-of-mass energy values used in our previous publications [4],[7] have since been corrected by +43 MeV due to a better understanding of the LEP energy scale.

From a fit to the cross sections for hadronic and leptonic decay modes as a function of energy, in the region of the Z^0 resonance, we determine the mass and total width of the Z^0 and its partial decay widths into hadrons and leptons. The invisible width is obtained from the difference between the measured total width and the sum of all observed partial widths. These results are compared with the expectations from the Standard Model.

2 The OPAL Detector

The data were recorded with the OPAL detector [8] at the CERN e^+e^- collider LEP. The tracking of charged particles was performed with a jet chamber, a large volume drift chamber divided into 24 azimuthal sectors with 159 layers of wires. The jet chamber, together with a vertex detector and a z-chamber, is positioned inside a solenoidal coil, which is surrounded by a time-of-flight counter array, a lead glass electromagnetic calorimeter with a presampler, an instrumented magnet return yoke serving as a hadron calorimeter and four layers of outer muon chambers. Forward detectors serve as a luminosity monitor.

The electromagnetic calorimeter, which played a central role in this analysis, consists of a cylindrical array of lead glass blocks, covering the region $|\cos\theta| < 0.82$, where θ is the angle with respect to the beam direction, and lead glass blocks in the endcaps, covering the region $0.81 < |\cos\theta| < 0.98$. The blocks each subtend a solid angle of approximately 40×40 mrad^2.

They project towards the interaction point in the barrel region and along the beam direction in the endcaps. The two sections of the electromagnetic calorimeter together cover 98% of the solid angle. The time-of-flight system (TOF) covers the region $|\cos\theta| < 0.82$ and consists of 160 scintillator bars. More details about the detector and the trigger have been given in [4,7].

For Monte Carlo studies the OPAL detector was simulated using a computer program [9], which includes the detector geometry and material as well as effects of resolution and efficiencies.

3 The Luminosity Measurement

The integrated luminosity of the colliding beams was determined by the measurement of small angle Bhabha scattering, a process insensitive to Z^0 effects. The measurement used the forward detector, consisting of two identical elements placed around the beam pipe at either end of the central tracking chambers. In this analysis two components of this detector were used in a complementary manner: (i) a calorimeter provided a high statistics measurement of the relative luminosity at each beam energy; (ii) a set of proportional tube chambers with a well defined geometry and acceptance provided the absolute luminosity calibration.

Each calorimeter consists of a cylindrical lead-scintillator sandwich divided into 16 azimuthal segments and two longitudinal sections: a presampler of 4 radiation lengths (X_0), and a main calorimeter of 22 X_0 [4]. For 45 GeV electrons, the energy resolution of the calorimeter was measured to be 1.3 GeV ($19\%\sqrt{E}$), with 84% of the energy deposited in the main calorimeter. Light sharing between adjacent segments and between inner and outer readouts of the main calorimeter was used to determine the center of the showers. The polar angle resolution varied between 1 and 10 mrad, being best near the inner edge of the calorimeter, while the resolution in azimuth varied between 3.5 and 35 mrad, being best at the segment boundaries. The acceptance of the calorimeter extends from 39 to 155 mrad, and is essentially complete in azimuth.

The proportional tube chambers are positioned between the presampler and main sections of the calorimeter. These chambers each consist of a vertical, horizontal, and diagonal plane of proportional tubes [10] of 1 cm^2 cross section. The positions of the centroids of showers from incident electrons or photons are measured using the pulse height information from the tubes. For 45 GeV electrons, the tube chambers have 1.3 mrad resolution in θ and ϕ and detect 99.3% of the showers. The tube chamber acceptance extends from 50 mrad to 135 mrad in polar angle, and covers 95% in azimuth. The positions of the tube chambers were surveyed to 1.0 mm and were checked with electron tracks measured in drift chambers [11] in front of the calorimeter.

To select events for the absolute luminosity calibration a fiducial region was defined well within the tube chamber and calorimeter acceptance, extending from 58 mrad to 124 mrad in polar angle from the nominal beam axis, and excluding azimuthal angles within 10 degrees of the horizontal and vertical planes. Particles emitted from the interaction point in this angular

region traversed only a minimum of material before reaching the forward detectors (less than 0.2 X_0). The average of the angles measured on the two sides of the event was required to lie within this fiducial region. Therefore the acceptance was largely independent of the position and size of the beam intersection region. To reject background due to off-momentum beam particles, the difference in the azimuthal angles between the two ends, $\Delta\phi$, was required to be in the range between 160° and 200°. Finally, the average of the energies of the largest cluster in each calorimeter was required to be larger than 2/3 of the beam energy. One quadrant of the tube chambers was not used since one segment in the corresponding calorimeter region was defective.

The detector read-out was triggered when the energy sum in each forward calorimeter exceeded 15 GeV overall, or 12 GeV in back-to-back clusters. The overall trigger efficiency was found to be 99.0 ± 0.3% for the events selected by these cuts. Figure 1 shows the energies measured in the two calorimeters for all events prior to the energy cut. The vertical and horizontal arms of the distribution correspond to radiative events in which one photon escapes undetected. A correction of 0.55%, with an uncertainty of 0.5%, was applied to account for the events that had a low measured energy at both ends of the detector. Most of these events were found to be small angle Bhabha events in which the electrons were outside the tube chamber acceptance but had showered into the fiducial volume.

The BABAMC Monte Carlo program [12] was used to generate $e^+e^- \rightarrow e^+e^-(\gamma)$ events, distributed at various energies across the Z^0 resonance. A Gaussian smearing of the angles and energies of the generated particles was introduced to simulate the effects of detector resolution seen in the data. Interference with the Z^0 changed the cross section for events within the tube chamber acceptance by a maximum of 1.0% from the simple $1/s$ QED dependence. The cross section corresponding to the selection criteria described above was calculated to be 18.17± 0.02 nb at the Z^0 peak. A theoretical systematic error of 1% was assigned to this calculation [13]. A 0.14% correction was applied to account for the contribution of the process $e^+e^- \rightarrow \gamma\gamma$. The radiative energy tails in figure 1 agreed well with the predictions of the Monte Carlo program. Throughout the fiducial region the measured average polar angles agreed well with the simulated distribution, which corresponds approximately to $1/\theta^3$, as shown in figure 2.

The sources of error in the absolute luminosity normalisation are detailed in table 1. The dominant contribution is the limited precision in the tube chambers survey, while further errors arise from small discrepancies between the data and the Monte Carlo prediction and residual uncertainties in determining the various correction factors. The final error of 2.2% includes a statistical error of 0.7% corresponding to 17,379 events in the calibration sample.

A check was made on the accuracy of the tube chamber luminosity calibration by using the shadow of the beam pipe support ring to establish a well defined inner edge for the calorimeter. This support is a precisely machined aluminium ring with a conical outer surface that points to the interaction region at a polar angle of 47 mrad. It has a thickness of two radiation lengths and is located 40 cm in front of the forward calorimeter. The addition of this material in front of the calorimeter alters the energy sharing between the presampler and the main calorimeter significantly. The energy deposited in the main calorimeter is about 15 GeV lower in the shadow of the beam pipe support ring than beyond it. This discontinuity of the

energy distribution in the main calorimeter accurately defines the edge of the acceptance at small θ. A measurement using this method, which is independent of the tube chambers, agreed with the tube chamber measurement to within $0.8 \pm 2.6\%$.

The relative luminosity between points of different beam energy was measured using the main calorimeters only. Events were selected in which the average energy of the largest clusters seen in the main sections of each calorimeter exceeded 70% of the beam energy. This requirement was high enough to eliminate the background, but was 3 standard deviations below the peak from well contained Bhabha events. It rejected Bhabha events only partially contained due to the radiation of an energetic photon or shower leakage at the edges of the calorimeter. To reduce backgrounds, the difference, $\Delta\phi$, in the azimuthal angles of the largest clusters was required to be in the range $160^\circ < \Delta\phi < 200^\circ$. A total of 58,124 events were selected by these cuts, of which less than 0.1% were background.

The energy calibration of the main calorimeter could be maintained to within 0.5% over the entire period of data taking. As a consequence, the cross section for luminosity events defined by these requirements was stable with time to within 0.8%. With an effective geometrical acceptance extending from 47 to 142 mrad in polar angle, the cross section was affected by Z^0 interference by at most 0.3%. Because the energy cut was imposed on the average of the energies in the two calorimeters, the acceptance was largely independent of beam displacements and the size of the beam intersection region.

The acceptance of the calorimeter selection was normalised to the tube chamber acceptance for a sample which included 70% of the data taking period. The Bhabha cross section for the calorimeter based luminosity measurement was thereby found to be 40.2 ± 0.9 nb at the Z^0 peak. The stability of the measurement was checked by comparing the tube chamber and calorimeter luminosities as a function of LEP fill and beam energy. No statistically significant systematic differences were observed. The beam energy dependent systematic error of the integrated luminosity was estimated to be 1% and was taken into account as a point-to-point systematic error in the cross section measurements.

The data recorded in 1989 correspond to an integrated luminosity of about $1.4 \mathrm{pb}^{-1}$. For the following analyses only those periods of data taking were used in which all detector components essential for the measurement were operating properly.

4 The Hadronic Decays

The criteria used to select hadronic Z^0 decays were nearly identical to the ones described in our previous publication [4]. The selection was mainly based on energy clusters in the electromagnetic calorimeter. Clusters in the barrel region were required to have an energy of at least 100 MeV, and clusters in the end cap were required to contain at least two adjacent lead glass blocks and have an energy of at least 200 MeV. The following three requirements defined a multihadron candidate: (i) at least 8 clusters, (ii) a total energy deposited in the lead glass of at least 10% of the centre-of-mass energy

$$R_{vis} = \Sigma E_{clus}/\sqrt{s} > 0.1,$$

where E_{clus} is the energy of each cluster, and (iii) an energy imbalance along the beam direction which satisfied

$$R_{bal} = \mid \Sigma(E_{clus} \cdot \cos\theta) \mid / \Sigma E_{clus} < 0.65.$$

The measured distributions of these variables are shown in figure 3. The cut on the number of clusters efficiently eliminated Z^0 decays into $e^+e^-$and $\tau^+\tau^-$. The R_{vis} cut discarded two-photon and beam-gas events. The cut in R_{bal} rejected beam-wall, beam-gas and beam-halo events, and cosmic rays in the end caps.

In order to reject cosmic ray background in the barrel region, information from the TOF counters was used. All events for which at least 4 TOF counters fired within 8 ns of the expected time were accepted. Events with less than 4 TOF counters for which at least 50% of the observed energy was seen in the barrel lead glass were rejected. All remaining events with $N_{TOF} < 4$ were visually inspected; this corresponded to less than 2% of all hadronic events. Out of this sample 36 events were rejected by the scan as being of cosmic-ray, beam-wall and beam-halo origin. The remaining background from each of these sources was estimated to be less than 0.1%. A total of 25,801 hadronic Z^0 decays remained after all these cuts, and the corresponding integrated luminosity was 1.25 pb^{-1}.

The main contamination in the hadronic data sample came from $\tau^+\tau^-$ events; a background fraction of $0.33 \pm 0.04\%$ was estimated by using Monte Carlo events generated with the KORALZ generator [14]. This estimate was checked with the data using the charged track multiplicity. The resulting background fraction was consistent with the Monte Carlo estimate. The contribution of the process $e^+e^- \rightarrow e^+e^-$ to the hadronic event sample was found to be less than 0.1%. The background from two-photon processes was estimated by a Monte Carlo calculation using a quark-parton model [15] and was checked with the data by measuring the ratio of the numbers of events with high and low R_{vis} as function of beam energy. Both estimates gave consistent results; the background was $0.03 \pm 0.03\%$ under the Z^0 peak and $0.2 \pm 0.2\%$ in the tail region.

To calculate the acceptance of the event selection procedure, the process $e^+e^- \rightarrow q\bar{q}$ with subsequent hadronisation was simulated using the JETSET parton shower model with five flavours and string fragmentation [16]. There is good agreement between the model predictions and the properties of the hadronic event sample (see for example figure 3 and reference [17]). An acceptance of 97.7% with a negligible statistical error was calculated for multihadronic events. Various checks were made to estimate the uncertainty in the acceptance calculation. The effect of uncertainties in the fragmentation model was estimated to be 0.5% by varying the parameters of the JETSET model and by using the HERWIG hadronisation model [18]. Imperfections in the detector simulation lead to a variation of the acceptance of 0.5%. The energy dependence of the acceptance in the region of the scan was 0.2%. The error due to the specific choice of the hadronic selection cuts was estimated to be 0.2%. The resulting total systematic error on the selection and acceptance of hadronic events was 0.8%.

The overall trigger efficiency for hadronic decays of the Z^0 that would pass the acceptance criteria was determined from the redundancy between the three main trigger modes: the TOF trigger, the track trigger and the electromagnetic energy trigger. For each trigger mode the efficiency was measured as a function of the direction of the thrust axis, θ_T. The resulting

overall trigger inefficiency in the region of $|\cos\theta_T| < 0.8$ was found to be less than 0.01%, while the inefficiency for events in forward direction, $|\cos\theta_T| > 0.8$, was less than 0.1% and therefore also negligible.

In table 2 the numbers of events, the integrated luminosities and the corresponding cross sections are listed as a function of the centre-of-mass energy. The error on the cross section includes the statistical errors of the hadronic event sample and of the luminosity as well as a 1% point-to-point systematic error from the luminosity. In the analysis of the cross section an overall normalisation error of 2.3% is taken into account which includes both the systematic error of 2.2% on the luminosity and the systematic error on the acceptance of 0.8%.

5 The Leptonic Decays

The criteria used to select $Z^0 \to e^+e^-$, $Z^0 \to \mu^+\mu^-$, and $Z^0 \to \tau^+\tau^-$ were similar to the ones described in detail in reference [7]. All three lepton-pair analyses were restricted to the region $|\cos\theta| < 0.7$ to ensure good trigger and reconstruction efficiencies.

The selection of e^+e^- events required two clusters in the barrel lead glass calorimeter, each with at least 50% of the beam energy and satisfying $|\cos\theta| < 0.7$; the acollinearity angle between these clusters (θ_{acol}) had to be less than 5°. The total reconstructed electromagnetic energy had to be greater than 85% of the centre-of-mass energy. All candidate events in the 90% of the data recorded when the jet chamber was at full operating voltage were visually scanned; it was required that the two highest energy clusters were associated with a charged track. A total of 29 events were rejected, coming mainly from $e^+e^- \to e^+e^-\gamma$ and $e^+e^- \to \gamma\gamma$ in which at least one of the two highest energy clusters was an isolated photon; this was consistent with the expected number of 26 events. After applying these cuts a sample of 908 events remained. A global efficiency of $98.8 \pm 0.8\%$ in the region $|\cos\theta| < 0.7$ was calculated using the BABAMC Monte Carlo program [12]. The efficiency contained contributions of $99.4 \pm 0.6\%$ from the cut on the total energy, $99.7 \pm 0.3\%$ from the effect of the angular resolution and the magnetic field on the acollinearity cut, and $99.7 \pm 0.2\%$ from the effect of the angular resolution on the $|\cos\theta| < 0.7$ cut. The background contamination in the final event sample was estimated to be $0.4 \pm 0.2\%$, arising from $\gamma\gamma$ and $e^+e^-\gamma$ events recorded when the central detector was off and from $\tau^+\tau^-$ events. The trigger efficiency was checked by comparing a number of independent triggers; it was found that the electromagnetic calorimeter trigger was 100% efficient for these events. Table 3 lists the number of events observed as a function of the centre-of-mass energy, together with the luminosity and the measured cross section in the range $|\cos\theta| < 0.7$. The total systematic error due to the uncertainty in the efficiency and background estimates is 0.9%.

Candidate $\mu^+\mu^-$ and $\tau^+\tau^-$ events were selected from a sample of events flagged by an online filter [7], and which in addition contained less than 13 lead glass clusters with energy above 250 MeV and less than 11 charged tracks with $p_T > 100$ MeV, where p_T is the momentum of the track in the plane perpendicular to the electron-positron beam direction.

Events were classified as $\mu^+\mu^-$ candidates if they contained at least two charged tracks

identified as muons. Both tracks had to satisfy the requirements: $p > 6$ GeV, $|\cos\theta| < 0.7$, and $d_0 < 1$ cm, where d_0 is the distance of closest approach of the track to the beam axis. The angle between the two tracks in ϕ had to be greater than 250 mrad. A track was classified as a muon if it satisfied any one of the following criteria: i) there were at least two hits in the barrel muon chambers associated with the track within $\Delta\phi = 70$ mrad, ii) within $\Delta\phi = 70$ mrad there was a track segment in the barrel hadron calorimeter, with hits in at least five of the nine layers, iii) the momentum was larger than 15 GeV and the sum of the energies in the barrel lead glass of all clusters within $\Delta\phi = 200$ mrad was less than 3 GeV. The efficiencies of these three criteria were $91.6 \pm 0.8\%$, $60.3 \pm 1.3\%$ and $92.5 \pm 0.7\%$, respectively.

Information from the TOF counters was used to remove the background from cosmic rays. Events were required to contain at least one TOF counter which measured a time within 10 ns of that expected for a particle coming from the interaction point. In addition, we considered the difference, Δt, between the times measured by pairs of TOF counters separated in azimuth by more than 165°; events in which $\Delta t > 10$ ns for all such pairs were rejected as cosmic rays. After applying these cuts a sample of 585 events remained, with a negligible background from cosmic rays.

Triggers for $\mu^+\mu^-$ events were provided by the central detector, the TOF counters, and the muon chambers. The resulting high degree of redundancy enabled the efficiencies of the individual components to be measured using the $\mu^+\mu^-$ events themselves. In this way the efficiency of the combined trigger was found to be $99.5 \pm 0.5\%$. By similar means the efficiency of the online filter was found to be $99.5 \pm 0.5\%$.

We evaluated the acceptance of the requirement that $\mu^+\mu^-$ events contain two tracks within $|\cos\theta| < 0.7$ to be $60.0 \pm 1.1\%$, using $\mu^+\mu^-$ events generated with the KORALZ Monte Carlo program [14] and then passed through the detector simulation. This program generates $e^+e^- \to \mu^+\mu^-$ and $e^+e^- \to \tau^+\tau^-$ according to the standard model, including the effects from initial and final state radiation. Using the same program, we calculated a background of $3.7 \pm 0.9\%$ from $Z^0 \to \tau^+\tau^-$ and from a Monte Carlo simulation [15] of $e^+e^- \to e^+e^-\mu^+\mu^-$ we calculated a background of $0.4 \pm 0.4\%$.

A number of systematic checks of the analysis were performed. From a search for $\mu^+\mu^-$ events in which one of the tracks in the central detector was not reconstructed we evaluated a track finding efficiency of $99.9 \pm 0.1\%$. The number of selected events was found to be insensitive to large changes in the cuts described above. These studies identified a number of imperfections in the simulation of the detector by the Monte Carlo program and we estimated an additional efficiency factor of $99 \pm 1\%$ to account for this fact. Taking into account the efficiency, acceptance and background we obtained an overall correction factor of 1.63 ± 0.04 for the number of $\mu^+\mu^-$ events.

The selection of $\tau^+\tau^-$ events relied mainly on the lead glass calorimeter and the jet chamber. The total electromagnetic energy observed in the lead glass had to be greater than 12 GeV and less than 70 GeV. A thrust axis was calculated from both the electromagnetic clusters and the charged tracks and was required to be in the angular range $|\cos\theta_T| < 0.7$. The event hemispheres defined by the plane perpendicular to the thrust axis were each required to have at least one and at most four charged tracks with $p_T > 100$ MeV and $d_0 < 3$ cm. Events

identified as $\mu^+\mu^-$ by the criteria described above were rejected, as were events identified as cosmic rays. Finally, a cut was made on the direction of the sum of the energy vectors measured in the lead glass with respect to the beam axis of $|\cos\theta| < 0.95$. This cut removed background from two-photon reactions and beam-gas interactions. After these cuts 506 events were left in our data sample. Figure 4 shows the energy distribution for events satisfying all cuts except the total energy cut and the $\mu^+\mu^-$ rejection.

The main trigger for these $\tau^+\tau^-$ events was the total energy trigger of the barrel lead glass, with a nominal threshold of 6 GeV. The overall trigger efficiency when combined with other, independent, triggers was 100%. The main on-line filter criterion was a requirement of a total energy of 8 GeV in the lead glass calorimeter, coincident with a TOF signal less than 27 ns after the beam crossing. The TOF requirement lead to a 1% inefficiency of this criterion. When combined with filter criteria independent of the TOF detector, the filter efficiency was 100%.

From the KORALZ program [14] we found that the geometrical acceptance for $\tau^+\tau^-$ events (requiring $|\cos\theta| < 0.7$) was 62.0 ± 1.5 %. The selection efficiency within the angular range was 76.3 ± 2.2 %, leading to an overall selection efficiency of 47.3 ± 2.0 %. The error in the acceptance was evaluated by varying the cuts and observing the change in the corrected number of events. We estimated the contribution from various background processes by subjecting samples of simulated background events to our selection program. The background channels considered were: $e^+e^- \rightarrow$ hadrons, $e^+e^- \rightarrow e^+e^-$, $e^+e^- \rightarrow \mu^+\mu^-\gamma$ and $e^+e^- \rightarrow e^+e^-X$. In total, the background in our final sample was estimated to be $6.2 \pm 2.2\%$. Taking into account the efficiency, acceptance and background we obtained an overall correction factor of 1.98 ± 0.10 for the number of $\tau^+\tau^-$ events.

Table 4 lists the number of $\mu^+\mu^-$ and $\tau^+\tau^-$ events observed as a function of centre-of-mass energy, together with the luminosity and the calculated cross section. We calculate a ratio of $\mu^+\mu^-$ to $\tau^+\tau^-$ decays of the Z^0 to be 0.96 ± 0.08, which is consistent with lepton universality. We also calculate a corrected number of Z^0 decays into $\mu^+\mu^-$ and $\tau^+\tau^-$ and multihadrons for the three energy points around the Z^0 peak; for this calculation we use a sample that satisfies the data quality requirements of all three analyses. In this sample we obtain the ratio of hadron to muon and tau decays at the peak of the Z^0: $N_{had}/N_{\mu\mu} = 22.2 \pm 1.2$ and $N_{had}/N_{\tau\tau} = 21.5 \pm 1.5$. Assuming lepton universality we obtain: $N_{had}/N_{l^+l^-} = 21.9 \pm 1.0$.

6 Analysis of the Hadronic Cross Section

To extract the Z^0 resonance parameters from the cross sections given in table 2 we perform a fit to the line shape parametrisation given in reference [19]. The line shape is described in terms of a resonance, an interference term and a pure QED term. Photonic corrections are treated in first order with exponentiation of soft photons. The contribution of the interference term is small over the energy range of the scan and is omitted in the fit as it would introduce an additional free parameter for each final state in a model independent approach. The approximation used has been compared to the full Standard Model calculation with second

order treatment of photonic corrections [20] and differs by less than 1.0% over the energy range of the scan.

We perform a model independent fit to the data based on reference [19], treating M_Z, Γ_Z and σ_{had}^{pole} as free parameters where σ_{had}^{pole} represents the resonance hadronic cross section at $s = M_Z^2$ without photonic corrections. The parameter values obtained are

$$M_Z = 91.145 \pm 0.022 \text{ (exp)} \pm 0.030 \text{ (LEP) GeV}$$

$$\Gamma_Z = 2.526 \pm 0.047 \text{ GeV}$$

$$\sigma_{had}^{pole} = 41.2 \pm 1.1 \text{ nb.}$$

The χ^2 value for this fit is 4.5 for 8 degrees of freedom. The errors on M_Z have been separated into the experimental error and the uncertainty due to the LEP beam energy. These results (summarized in table 5 column 1) can be compared with our previous measurement [4]: $M_Z = 91.05 \pm 0.05$ (exp) ± 0.05 (LEP) GeV, $\Gamma_Z = 2.60 \pm 0.13$ GeV and $\sigma_{had}^{pole} = 41.7 \pm 2.4$ nb, where the mass value has been corrected for the new energy calibration of LEP. Figure 5 shows the central values and the confidence contours for our measurement of Γ_Z and σ_{had}^{pole}.

The Standard Model predictions for the pole cross section σ_{had}^{pole}, the width Γ_Z and the partial decay widths discussed below are a function of M_Z and depend on the values assumed for the top quark mass m_t, the Higgs mass m_H and the strong coupling constant α_s. In order to compare our measurement with the Standard Model predictions we calculate those assuming $m_t = m_H = 100$ GeV, and setting $\alpha_s = 0.12$, consistent with the value derived from the measured hadronic jet production rates [21]. The errors on the predictions are derived by allowing a variation of m_t from 50 to 250 GeV, m_H from 20 to 1000 GeV and α_s from 0.09 to 0.15.

Figure 5 shows that the effect of varying the number of light neutrino generations from 3 to 4 is large compared to the uncertainty in the predicted values of σ_{had}^{pole} and Γ_Z. The probability for obtaining our measurement assuming three neutrinos is 54% whereas the assumption of four neutrinos would result in a probability of only 0.001%.

The number of light neutrinos, N_ν, can also be found by using the Standard Model in a fit where the only other free parameter is M_Z. In this fit, the total width and hadronic pole cross section are parametrised by

$$\Gamma_Z = \Gamma_{had}^{SM} + 3\Gamma_e^{SM} + N_\nu \Gamma_\nu^{SM} \quad \text{and} \quad \sigma_{had}^{pole} = \frac{12\pi}{M_Z^2} \frac{\Gamma_e^{SM} \Gamma_{had}^{SM}}{\Gamma_Z^2}.$$

Here, $\Gamma_{had}^{SM} = 1734^{+47}_{-21}$ MeV, $\Gamma_e^{SM} = 83.4^{+1.3}_{-0.6}$ MeV and $\Gamma_\nu^{SM} = 166.2^{+2.7}_{-0.7}$ MeV are the Standard Model predictions for the partial width for hadrons, electrons and for each light neutrino. The two parameter fit yields

$$M_Z = 91.141 \pm 0.022 \text{ (exp)} \pm 0.030 \text{ (LEP) GeV}$$

$$N_\nu = 3.09 \pm 0.19 \text{ (exp)}^{+0.06}_{-0.12} \text{ (theor)}$$

with a χ^2 of 5.5 for 9 degrees of freedom.

Though this method to determine the number of light neutrinos is the statistically most precise one, it relies on the validity of the Standard Model prediction for all the Z^0 partial widths. This constraint can be removed by a measurement of the hadronic and the leptonic partial widths.

7 Combined Analysis of Hadrons and Leptons

In the following we describe how M_Z, Γ_Z and the partial widths Γ_e, Γ_μ, Γ_τ and Γ_{had} are determined, in a model independent way, from our measurement of the line shapes for the four processes $e^+e^- \rightarrow$ hadrons, e^+e^-, $\mu^+\mu^-$, and $\tau^+\tau^-$.

The systematic uncertainties of the decay widths are highly correlated. Normalisation and point-to-point energy scale uncertainties are completely correlated for the four channels. Further correlations are introduced by the ratio $\Gamma_e/(M_Z^2 \cdot \Gamma_Z^2)$ used in extracting the four partial widths from the measured cross sections. We therefore perform a combined fit to the four line shapes, based on a χ^2-minimisation which takes into account the full covariance matrix of the data. This procedure allows us to take into account all systematic errors on the cross sections mentioned above as well as their correlations. The uncertainties of all parameters can therefore be determined correctly. Because of the implicit assumption of Gaussian probability distributions, this method precludes the use of low statistics data points. For the lepton analysis data points have been discarded if the Standard Model prediction amounts to less than 10 observed events for the measured luminosity. The fitting procedure was checked using a maximum likelihood method.

For all final states excluding the e^+e^- channel, we use the line shape parametrisation as described in [19]. Due to the presence of the t-channel the cross-section for $e^+e^- \rightarrow e^+e^-$ diverges if no angular cut is applied. For the e^+e^- final state, however, the effect of an angular cut strongly depends on the resonance parameters. We therefore use in our fit a parametrisation of the differential cross section which is integrated for each choice of parameters in the angular range of the measured data. This parametrisation, described in [22], is based on the line shape program BHABHA [23] which uses the formalism developed in [24]. The program accounts for γ- and Z-exchange in s- and t-channel and all possible interference terms. Photonic corrections are treated in a first order calculation with exponentiation of soft photons. Hard photons are treated in the collinear approximation. The t-channel effects are large: the peak cross section is enhanced by approximately 15% for $|\cos\theta| < 0.7$ and the line shape significantly distorted with respect to the pure s-channel process.

The program requires the specification of kinematic cuts on the photon energy(k) and the opening angle(δ) between the hard photon and the final-state electron or positron. Our measured cross section, however, is obtained by requiring that the acollinearity angle (θ_{acol}) between electron and positron is smaller than 5°. In order to compare the results of the theoretical calculation with our measurement we have used cuts on k and δ that give the best approximation to the kinematic region $\theta_{acol} < 5°$, namely $k < 0.083 \cdot E_{beam}$ and $\delta < 5°$. We have applied a correction factor to the data to account for the fact that the two kinematic regions are not precisely the same. This factor has been calculated by using the program

BHABHA iteratively and varies from -1.6% to -2.3% over the energy range of the scan. As a check this correction factor has also been calculated using the BABAMC Monte Carlo program [12]. The two methods agree to approximately 1% near the Z^0 peak. There is another correction to be made to the data in order to compensate for the loss due to acollinear events near to the boundary of the acceptance at $|\cos\theta| = 0.7$. This correction has also been estimated using the BABAMC Monte Carlo at each point of the energy scan: it ranges from 0.5 to 1.5%. The corrected cross sections are listed in the last column of table 3. The systematic error in the calculation of the cross section for the process $e^+e^- \rightarrow e^+e^-$ by the program BHABHA, with the cuts $k < 0.083 \cdot E_{beam}$ and $\delta < 5°$, was estimated to be 2.5% by comparing the results of the line shape program with those of the BABAMC program. Because the exponentiation of soft photons is not performed in BABAMC, for the purpose of this comparison we did not use exponentiation in the line shape program; no systematic error has been assigned to the exponentiation procedure used in the BHABHA program. When combined with the experimental uncertainty of 0.9% on the efficiency and background estimates, the total systematic error of the corrected Bhabha cross section is 2.7%.

The line shapes resulting from the combined fit are shown in figure 6, superimposed on the data. The parameter values for this fit are summarised in table 5 column 2. As expected, the values of M_Z, Γ_Z and $\sigma^{\rm pole}_{\rm had}$, as obtained from the combined fit, agree well with those derived from the hadronic data alone. The leptonic widths we observe are consistent with lepton universality. We therefore repeat the fit constraining all leptonic widths to be equal. The result of this fit is given in table 5 column 3. A combined fit can also be used to determine the decay branching ratios of the Z^0, the results are summarised in table 6.

In table 5 column 4 the Standard Model expectation for the leptonic, hadronic and total widths are given for our measured value of the Z^0 mass, with the assumption of three neutrino generations. It can be seen that the measured total width is larger than the expectation by more than one standard deviation, and that the hadronic width is larger by more than two standard deviations, whereas the leptonic width is in good agreement but somewhat smaller than the predicted value. By examining the χ^2 behaviour of the combined fit we establish an overall probability of 6% for observing such deviations, assuming the Standard Model with the above parameters.

In order to study the dependence of the results on the values assumed for the top quark mass and the strong coupling constant, we vary m_t between 50 and 250 GeV and α_s between 0.09 and 0.15, setting m_H to 20 GeV. The deviation of the Standard Model prediction from our measurement is minimized when we set both, m_t and α_s, to the maximum value of the specified ranges. With this assumption we would have assigned a probability of 25% to our results. In this estimate QCD corrections up to second order to the hadronic partial width were taken into account. The inclusion of the third order perturbative coefficient [25] alters these corrections from about 4% (in second order) to 4.4 % for $\alpha_s = 0.12$; this increases the calculated hadronic width by 7 MeV.

The Standard Model partial widths all increase appreciably with increasing top mass. Figure 7 shows our measurements of the hadronic and leptonic partial widths; also indicated is the uncertainty of the Standard Model prediction with the parameter range considered here. In the ratio of the partial widths the dependence on the top quark mass is reduced.

In particular, the allowed range of values for the ratio of the hadronic to the leptonic partial width, R_Z^{SM}, is

$$20.6 \leq R_Z^{SM} = \frac{\Gamma_{had}^{SM}}{\Gamma_{l^+l^-}^{SM}} \leq 21.1,$$

where the range of R_Z^{SM} reflects mainly the uncertainty assigned to α_s in second order QCD. The ratio R_Z has the additional feature that some experimental systematic errors cancel; in particular it is independent of the absolute luminosity measurement. Our determination of R_Z, from the combined fit, is

$$R_Z = \frac{\Gamma_{had}}{\Gamma_{l^+l^-}} = 22.43 \pm 0.75.$$

The value of R_Z is in agreement with the corrected ratio of the number of hadronic to $\mu^+\mu^-$ and $\tau^+\tau^-$ events, observed near the peak, $(N_{had}/N_{l^+l^-}) \cdot f = 22.1 \pm 1.0$, where the factor $f = 1.013$ accounts for photon exchange in the s-channel. Within the parameter range considered here our measurement of R_Z differs from the Standard Model prediction by 1.8 to 2.4 standard deviations.

The results from the combined fit can also be expressed as a model independent measure of the invisible width by the relation,

$$\Gamma_{inv} = \Gamma_Z - 3\Gamma_{l^+l^-} - \Gamma_{had}.$$

We obtain

$$\Gamma_{inv} = 453 \pm 44 \text{ MeV}.$$

Based on the Standard Model value of Γ_ν^{SM} given above, we obtain,

$$\frac{\Gamma_{inv}}{\Gamma_\nu^{SM}} = N_\nu = 2.73 \pm 0.26(\text{exp})^{+0.02}_{-0.04}(\text{theor}).$$

This measurement of the invisible width excludes four generations of light neutrinos with Standard Model couplings by more than 4 standard deviations. The measurement lies below the Standard Model prediction for three generations with light neutrinos by about one standard deviation. This observation should not, however, be considered independently of the deviation of R_Z discussed above.

8 Summary

We have measured the production and decay of the Z^0 into hadrons and leptons. The results presented here are based on 25,801 hadronic decays and 1999 leptonic decays collected during a scan around the Z^0 resonance.

We have fit the Z^0 lineshape parameters using the combined hadronic and leptonic data. From this fit we determine the Z^0 mass to be $M_Z = 91.154 \pm 0.021 \pm 0.030$ GeV, its total width $\Gamma_Z = 2.536 \pm 0.045$ GeV, and the leptonic widths $\Gamma_{ee} = 81.2 \pm 2.6$ MeV, $\Gamma_{\mu\mu} = 82.6 \pm 5.8$ MeV, $\Gamma_{\tau\tau} = 85.7 \pm 7.1$ MeV. We find good agreement with lepton universality; performing a fit

with this constraint imposed, we obtain for the leptonic width $\Gamma_{l^+l^-} = 81.9 \pm 2.0$ MeV and for the hadronic width $\Gamma_{had} = 1.838 \pm 0.046$ GeV.

In the Standard Model the ratio $R_Z = (\Gamma_{had}/\Gamma_{l^+l^-})$ depends only weakly on the assumed values of the top quark and Higgs masses. The predicted value for R_Z lies between 20.6 and 21.1 where the range mainly reflects the uncertainty in α_s. From the combined fit we obtain a value $R_Z = 22.43 \pm 0.75$ which differs from the Standard Model prediction by approximately two standard deviations.

The invisible width, determined by subtracting the hadronic and three times the leptonic partial width from the total width is found to be $\Gamma_{inv} = 453 \pm 44$ MeV. By using the Standard Model width to neutrinos we obtain $N_\nu = 2.73 \pm 0.26(\mathrm{exp})^{+0.02}_{-0.04}(\mathrm{theor})$. This measurement excludes four generations of light neutrinos with Standard Model couplings by more than four standard deviations.

9 Acknowledgements

It is a pleasure to thank the LEP Division for the efficient operation of the machine, the precise information on the absolute energy, and their continuing close cooperation with our experimental group. In addition to the support staff at our own institutions we are pleased to acknowledge the following: The Bundesministerium für Forschung und Technologie, FRG, The Department of Energy, USA, The Institut de Recherche Fondamentale du Commissariat a l'Energie Atomique, The Israeli Ministry of Science, The Minerva Gesellschaft, The National Science Foundation, USA, The Natural Sciences and Engineering Research Council, Canada, The Japanese Ministry of Education, Science and Culture (the Monbusho) and a grant under the Monbusho International Science Research Program, The Science and Engineering Research Council, UK and The A. P. Sloan Foundation.

References

[1] G.S. Abrams et al., Phys. Rev. Lett. 63 (1989) 724,
G.S. Abrams et al., Phys. Rev. Lett. 63 (1989) 2173

[2] L3 Collaboration, B. Adeva et al., Phys. Lett. B231 (1989) 509

[3] ALEPH Collaboration, D. Decamp et al., Phys. Lett. B231 (1989) 519

[4] OPAL Collaboration, M.Z. Akrawy et al., Phys. Lett. B231 (1989) 530

[5] DELPHI Collaboration, P. Aarnio et al., Phys. Lett. B231 (1989) 539

[6] ALEPH Collaboration, D. Decamp et al., Phys. Lett. B235 (1990) 399
L3 Collaboration, B. Adeva et al., L3 preprint 4, Dec. 1989, submitted to Phys. Lett.
L3 Collaboration, B. Adeva et al., L3 preprint 5, Feb. 1990, submitted to Phys. Lett.

[7] OPAL Collaboration, M.Z. Akrawy et al., Phys. Lett. B235 (1990) 379

[8] OPAL Technical proposal (1983) and CERN/LEPC/83-4, and
OPAL Collaboration, K. Ahmet et al., The OPAL Detector at LEP, to be submitted to Nucl. Instr. and Meth.

[9] J. Allison et al., Comp. Phys. Comm. 47 (1987) 55;
R. Brun et al., GEANT 3, Report DD/EE/84-1, CERN (1989).

[10] D.C.Imrie, et al, Nucl.Inst. and Meth. A283 (1989) 515

[11] B.E.Anderson, et al, Nucl.Inst. and Meth. A283 (1989) 650

[12] M. Böhm, A. Denner and W. Hollik, Nucl. Phys. B304 (1988) 687
F.A. Berends, R. Kleiss, W. Hollik, Nucl. Phys. B304 (1988) 712

[13] R. Kleiss et al., Z Physics at LEP1, CERN 89-08, ed. G. Altarelli et al., Vol 3 (1989) 126

[14] S. Jadach et al., Z Physics at LEP1, CERN 89-08, ed. G. Altarelli et al., Vol 1 (1989); KORALZ, Version 37

[15] F.A.Berends, P.H.Daverveldt and R.Kleiss, Comp. Phys. Comm. 40 (1986) 271, 285, 309.

[16] T. Sjöstrand, Comp. Phys. Comm. 39 (1986) 347; JETSET, Version 7.1.

[17] OPAL Collaboration, M.Z. Akrawy et al., Phys. Lett. B236 (1990) 364

[18] G. Marchesini and B.R. Webber, Nucl. Phys. B310 (1988) 461; HERWIG, Version 3.2.

[19] D. Bardin et al., Z Physics at LEP1, CERN 89–08, ed. G.Altarelli et al., Vol.1 (1989) 89.

[20] Line shape program ZSHAPE: W.J.P. Beenakker, F.A. Berends and S.C. van der Marck (Instituut–Lorentz, University of Leiden, POB 9506, 2300 RA Leiden, The Netherlands)

[21] OPAL Collaboration, M.Z. Akrawy et al., Phys. Lett. B235 (1990) 389

[22] M.Caffo, E.Remiddi and F.Semeria, Z Physics at LEP1, CERN 89−08, ed. G.Altarelli et al., Vol.1 (1989) 171.

[23] Program BHABHA from M. Caffo, E. Remiddi and F. Semeria

[24] M. Greco, Phys. Lett. B177 (1986) 97

[25] Z. Kunszt and P. Nason, Z Physics at LEP1, CERN 89−08, ed. G.Altarelli et al., Vol.1 (1989) 373.

Figure Captions

Figure 1: The energies measured in the two forward calorimeters, E_1 vs E_2, for luminosity event candidates passing the tube chamber selection cuts. The shaded region is excluded by the trigger requirement that at least 12 GeV be deposited in opposite calorimeter segments. Events in the region above the diagonal satisfy the requirement that 2/3 of the centre-of-mass energy is observed in the calorimeter.

Figure 2: Angular distribution of luminosity event candidates, as measured by the tube chambers. The arrows show the boundaries of the fiducial region, inside of which the data follow the expected $1/\theta^3$ distribution, shown by the curve.

Figure 3: The measured distributions of the variables used in the selection of hadronic events, each shown after applying all other cuts: (a) Number of clusters in the electromagnetic calorimeter, (b) Visible fraction of centre-of-mass energy, R_{vis} (see text), (c) Longitudinal energy imbalance R_{bal} (see text). The simulated distributions using a QCD parton shower model are also shown. The arrows indicate the cuts applied.

Figure 4: Observed energy distribution of τ-candidates after all cuts were applied except the energy cut and the $\mu^+\mu^-$ rejection. The open histogram is a Monte Carlo simulation of $\tau^+\tau^-$ events, the shaded histograms at the left and right are simulations of $\mu^+\mu^-$ and e^+e^- events respectively. All Monte Carlo distributions are generated using the Standard Model leptonic decay width.

Figure 5: The confidence contours in the Γ_Z - σ_{had}^{pole} plane. Shown are the one, two and three standard deviation contours of our measurement. The small square shows the best fit to the data; the circle shows the Standard Model prediction for 3 light neutrino generations, the large square the prediction for 4 neutrinos. The bars reflect the uncertainty in the predictions when the top quark mass is varied from 50 to 250 GeV, the Higgs mass from 20 to 1000 GeV and α_s between 0.09 and 0.15.

Figure 6: Measured cross sections at the 11 points of the scan for (a) $e^+e^- \rightarrow$ hadrons, (b) e^+e^- in the range of $|\cos\theta| < 0.7$, (c) $\mu^+\mu^-$, and (d) $\tau^+\tau^-$. Also shown are the line shapes from the combined fit to all data. The open circles indicate points not used in the fit (see text). The dashed curve, shown in (a) together with the hadronic data, is the line shape predicted by the Standard Model assuming the measured M_Z and 4 neutrino generations.

Figure 7: The confidence contours in the Γ_{had} - $\Gamma_{l^+l^-}$ plane. Shown are the one and two standard deviation contours of our measurement. The small dot shows the best fit to the data; the large dot shows the standard model predictions for 3 light neutrino generations, the line reflects the uncertainty in the predictions when the top quark mass is varied from 50 to 250 GeV, and the Higgs mass from 20 to 1000 GeV. The shaded area indicates the effect on Γ_{had} of also varying α_s between 0.09 and 0.15.

Source of Error	Magnitude
Theory	1%
Radial survey	1.5%
Efficiency of tube chambers	0.5%
Trigger efficiency	0.3%
Energy cut	0.5%
Radial cut	0.5%
Background subtraction	0.5%
Total systematic error	2.1%
Statistical error	0.7%
Total uncertainty	2.2%

Table 1: Contributions to the absolute luminosity measurement uncertainty. The systematic errors contributing to the overall uncertainty are listed and then combined with the statistical error.

$\sqrt{s}$ (GeV)	$\mathcal{L}_{\rm int}$(nb^{-1})	$N_{\rm had}$	$\sigma_{\rm had}$ (nb)
88.278	115.1±1.6	569	5.04 ± 0.23
89.283	80.7±1.4	766	9.68 ± 0.40
90.284	103.7±1.6	1990	19.56 ± 0.56
91.034	210.9±2.3	6192	29.94 ± 0.58
91.289	186.2±2.1	5633	30.86 ± 0.62
91.529	230.8±2.4	6612	29.21 ± 0.55
92.282	85.5±1.5	1781	21.24 ± 0.66
92.562	9.2±0.5	150	16.66 ± 1.62
93.286	111.4±1.7	1286	11.77 ± 0.39
94.277	95.4±1.6	710	7.59 ± 0.32
95.036	17.7±0.7	112	6.44 ± 0.66
Total	1246.6	25801	

Table 2: The hadronic cross section, $\sigma_{\rm had}$, as a function of the luminosity-weighted centre-of-mass energy, $\sqrt{s}$. Listed are also the integrated luminosity $\mathcal{L}_{\rm int}$ and the number of observed hadronic events $N_{\rm had}$. The cross sections are quoted with their statistical and point-to-point systematic luminosity error of 1%. The overall systematic error on the cross section is 2.3 % and on the energy scale is 30 MeV. The point-to-point error on the energy is 10 MeV.

$\sqrt{s}$ (GeV)	$\mathcal{L}_{\rm int}$ ($\rm nb^{-1}$)	$N^{obs}_{e^+e^-}$	$\sigma^{meas}_{e^+e^-}$(nb) $\lvert\cos\theta\rvert < 0.7$	$\sigma^{corr}_{e^+e^-}$(nb) $\lvert\cos\theta\rvert < 0.7$
88.279	116.3 ± 1.6	30	0.260 ± 0.048	0.256 ± 0.047
89.285	66.8 ± 1.3	30	0.453 ± 0.083	0.445 ± 0.082
90.284	118.0 ± 1.7	78	0.666 ± 0.076	0.655 ± 0.075
91.035	231.3 ± 2.4	202	0.880 ± 0.063	0.864 ± 0.061
91.287	251.0 ± 2.5	237	0.952 ± 0.063	0.935 ± 0.061
91.530	236.3 ± 2.4	210	0.896 ± 0.062	0.880 ± 0.061
92.285	76.8 ± 1.4	41	0.538 ± 0.085	0.530 ± 0.083
92.563	10.1 ± 0.5	2	0.199 ± 0.141	0.196 ± 0.139
93.285	117.2 ± 1.7	45	0.387 ± 0.058	0.383 ± 0.057
94.282	92.0 ± 1.6	28	0.307 ± 0.058	0.305 ± 0.058
95.036	19.0 ± 0.7	5	0.266 ± 0.119	0.265 ± 0.119
Total	1334.8	908		

Table 3: The measured cross section, $\sigma^{meas}_{e^+e^-}$ for the reaction $e^+e^- \to e^+e^-$, in the region $\lvert\cos\theta\rvert < 0.7$ and acollinearity angle $\theta_{acol} < 5°$, as a function of the luminosity-weighted centre-of-mass energy. Listed are also the integrated luminosities $\mathcal{L}_{\rm int}$, the event counts $N^{obs}_{e^+e^-}$ and the corrected cross sections $\sigma^{corr}_{e^+e^-}$ (see text). The errors quoted are statistical only.

$\sqrt{s}$ (GeV)	$\mathcal{L}_{\rm int}(\mu^+\mu^-)$ ($\rm nb^{-1}$)	$N^{obs}_{\mu^+\mu^-}$	$\sigma_{\mu^+\mu^-}$ (nb)	$\mathcal{L}_{\rm int}(\tau^+\tau^-)$ ($\rm nb^{-1}$)	$N^{obs}_{\tau^+\tau^-}$	$\sigma_{\tau^+\tau^-}$ (nb)
88.280	113.6 ± 1.6	20	0.29 ± 0.06	120.1 ± 1.7	15	0.25 ± 0.06
89.280	43.6 ± 1.0	8	0.30 ± 0.11	45.9 ± 1.0	10	0.43 ± 0.14
90.279	78.6 ± 1.4	42	0.87 ± 0.14	80.4 ± 1.4	43	1.06 ± 0.16
91.034	157.9 ± 2.0	119	1.23 ± 0.11	169.9 ± 2.0	132	1.54 ± 0.14
91.285	163.2 ± 2.0	144	1.44 ± 0.12	136.9 ± 1.8	98	1.42 ± 0.14
91.530	193.6 ± 2.2	160	1.35 ± 0.11	203.7 ± 2.2	132	1.29 ± 0.11
92.281	53.6 ± 1.2	34	1.04 ± 0.18	55.5 ± 1.2	18	0.64 ± 0.15
92.564	5.4 ± 0.4	1	0.30 ± 0.30	6.1 ± 0.4	2	0.65 ± 0.46
93.280	85.3 ± 1.5	30	0.57 ± 0.11	84.1 ± 1.5	28	0.66 ± 0.13
94.282	79.9 ± 1.5	22	0.45 ± 0.10	83.9 ± 1.5	23	0.54 ± 0.11
95.036	13.9 ± 0.6	5	0.59 ± 0.26	16.6 ± 0.7	5	0.60 ± 0.27
Total	988.6	585		1003.1	506	

Table 4: The cross sections of the reactions $e^+e^- \to \mu^+\mu^-$ and $e^+e^- \to \tau^+\tau^-$ as a function of the luminosity-weighted centre-of-mass energy. Listed are also the integrated luminosities and the event counts. The errors quoted are statistical only.

	hadronic data only	all data without lepton universality	all data with lepton universality	SM expectation m_t=m_H=100GeV $\alpha_s = 0.12$
M_Z [GeV]	91.145±0.022	91.154±0.021	91.154±0.021	91.154 (input)
Γ_Z [GeV]	2.526±0.047	2.536±0.045	2.536±0.045	2.483
σ^{pole}_{had} [nb]	41.2±1.1	41.4±1.1	41.4±1.1	41.4
Γ_{ee}[MeV]		81.2±2.6		
$\Gamma_{\mu\mu}$[MeV]		82.6±5.8		
$\Gamma_{\tau\tau}$[MeV]		85.7±7.1		
$\Gamma_{l^+l^-}$[MeV]			81.9±2.0	83.4
Γ_{had}[GeV]		1.854±0.058	1.838±0.046	1.734
Γ_{inv}[MeV]		433±61	453±44	499
χ^2 /NDOF	4.5/5	30.8/32	31.2/34	

Table 5: Results of the fit to the hadronic data and of the combined fit to the hadronic and leptonic data. M_Z has an additional error of 30 MeV from the energy uncertainty. The fourth column indicates the Standard Model expectations assuming our measured Z^0 mass, 3 generations of light neutrinos, top quark and Higgs masses set to 100 GeV and α_s to 0.12.

	Decay channel	Branching ratio
	e^+e^-	3.20 ± 0.09
	$\mu^+\mu^-$	3.26 ± 0.18
	$\tau^+\tau^-$	3.38 ± 0.25
assuming lepton	l^+l^-	3.23 ± 0.06
universality:	hadrons	72.5 ± 1.7
	invisible	17.9 ± 1.6

Table 6: Branching ratios for the decays of the Z^0 (%). Lepton universality is assumed in the calculation of the hadronic and invisible branching ratios

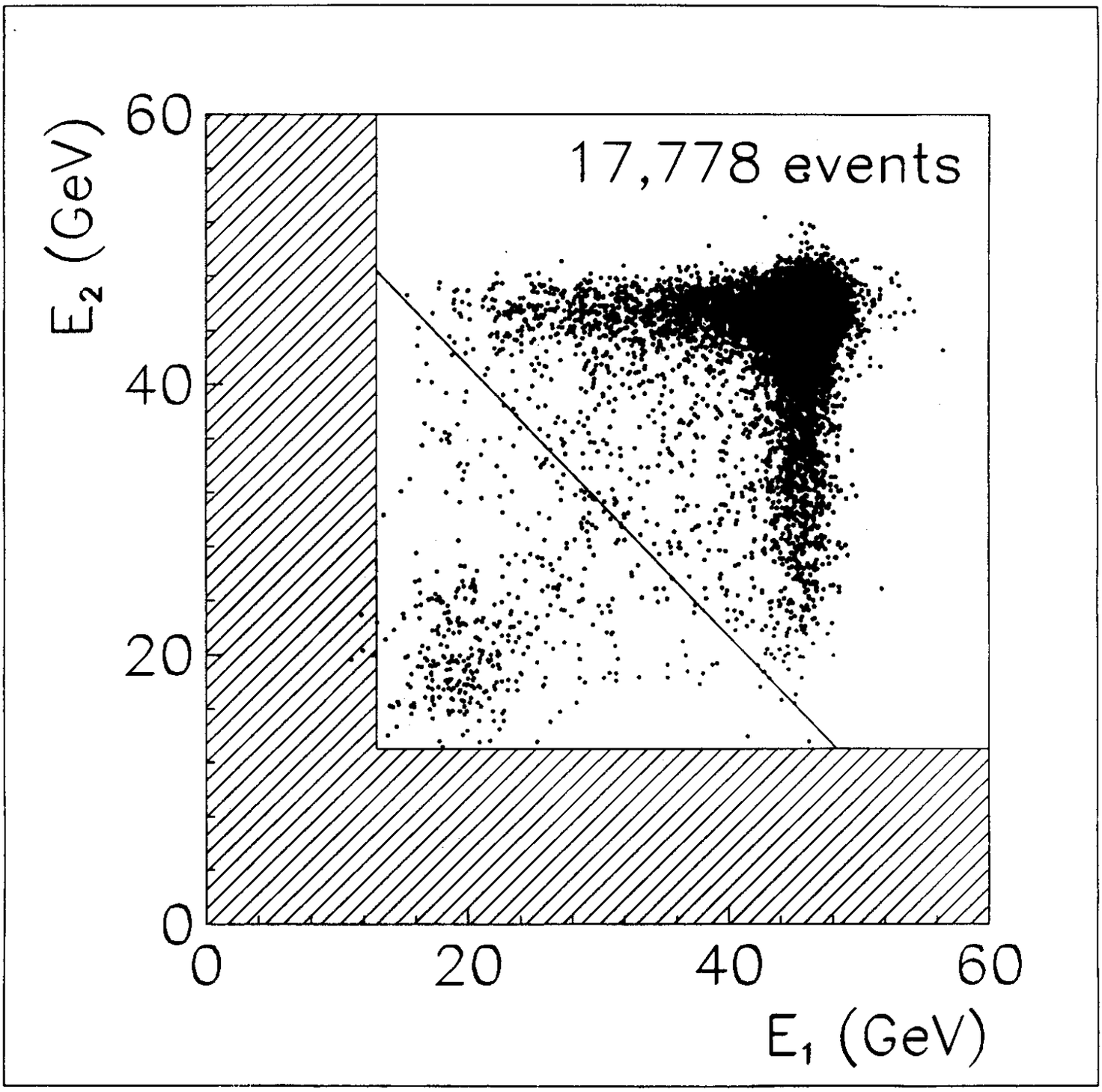

FIG. 1

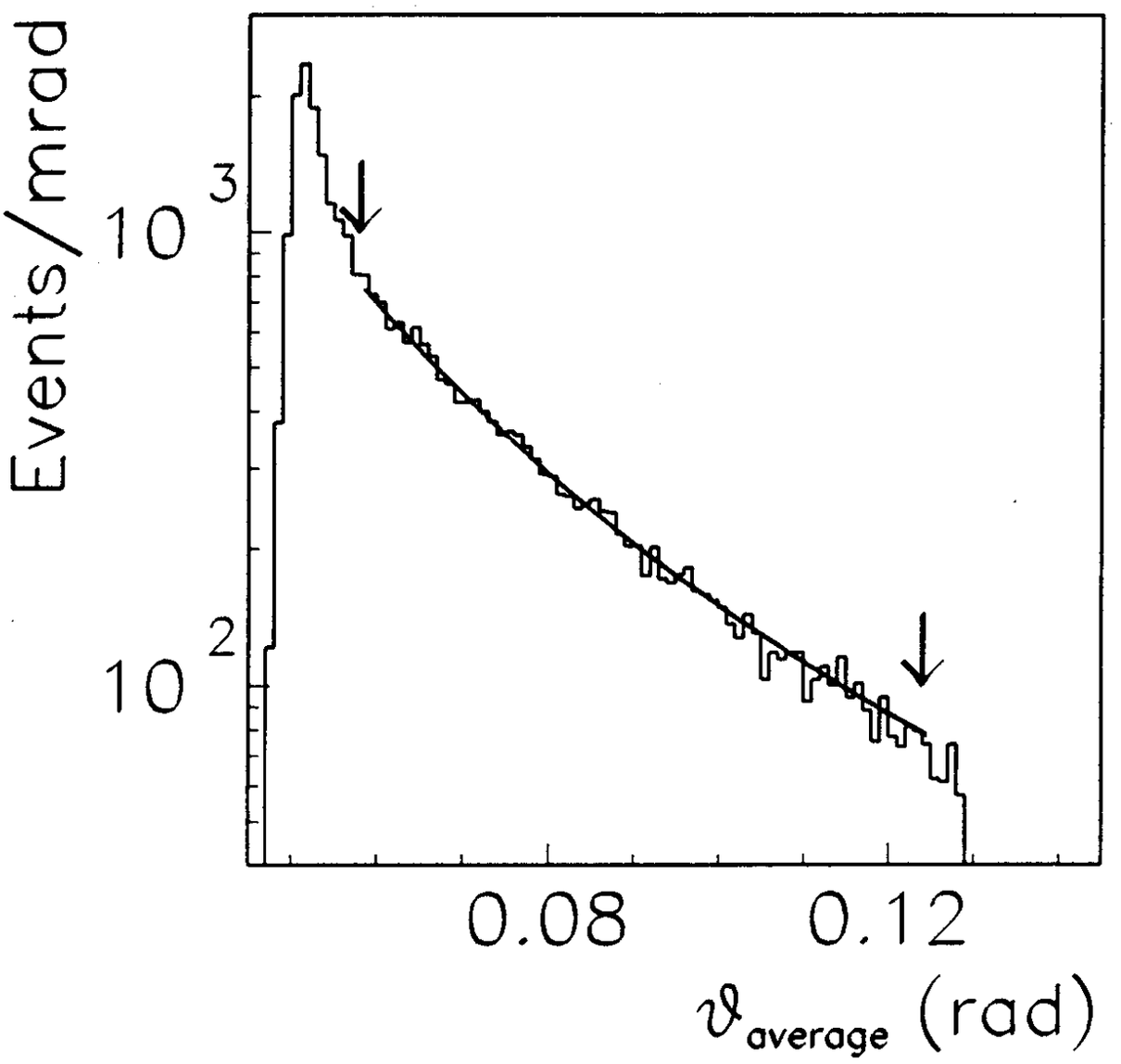

FIG. 2

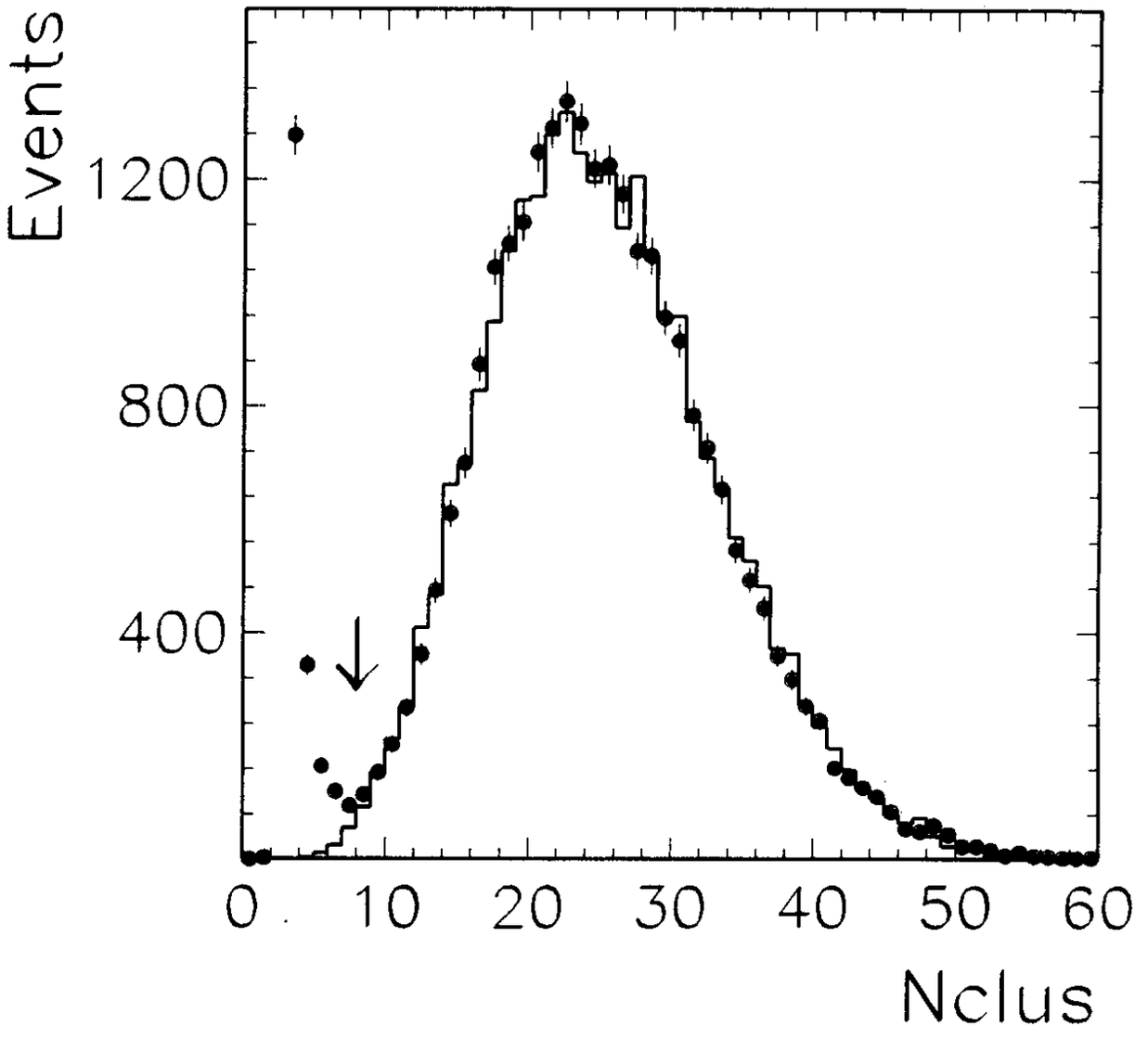

FIG. 3a

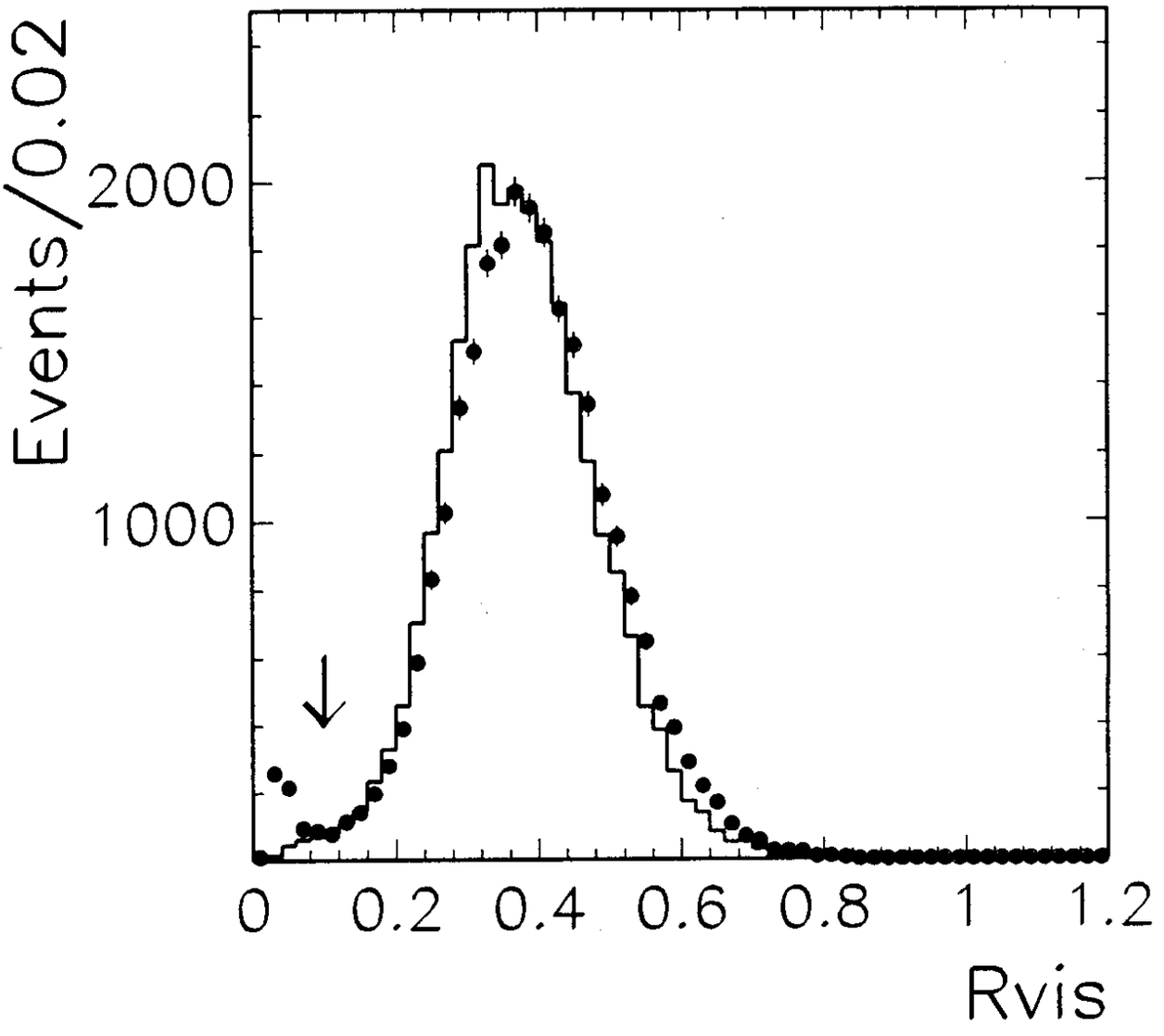

FIG. 3b

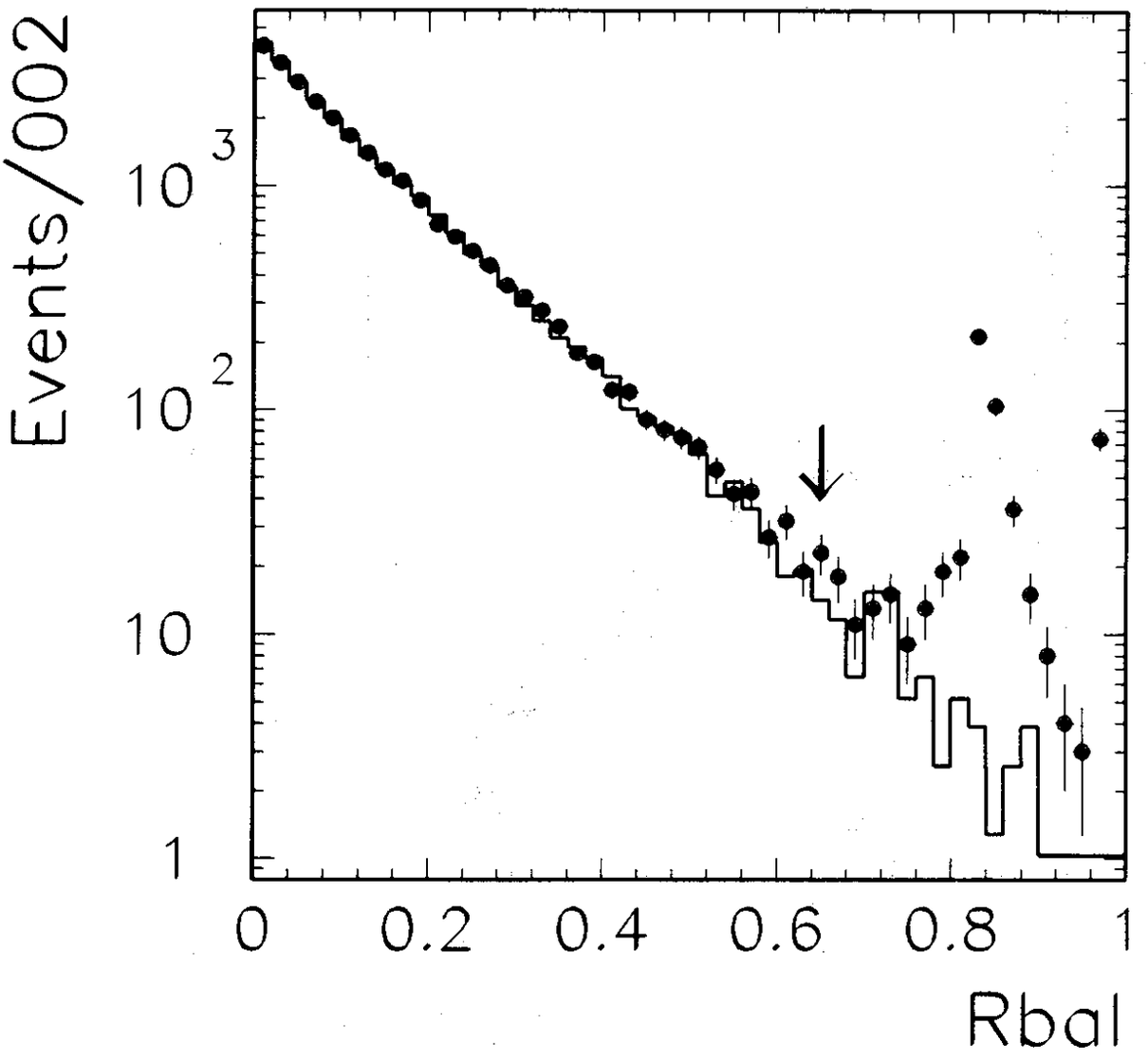

FIG. 3c

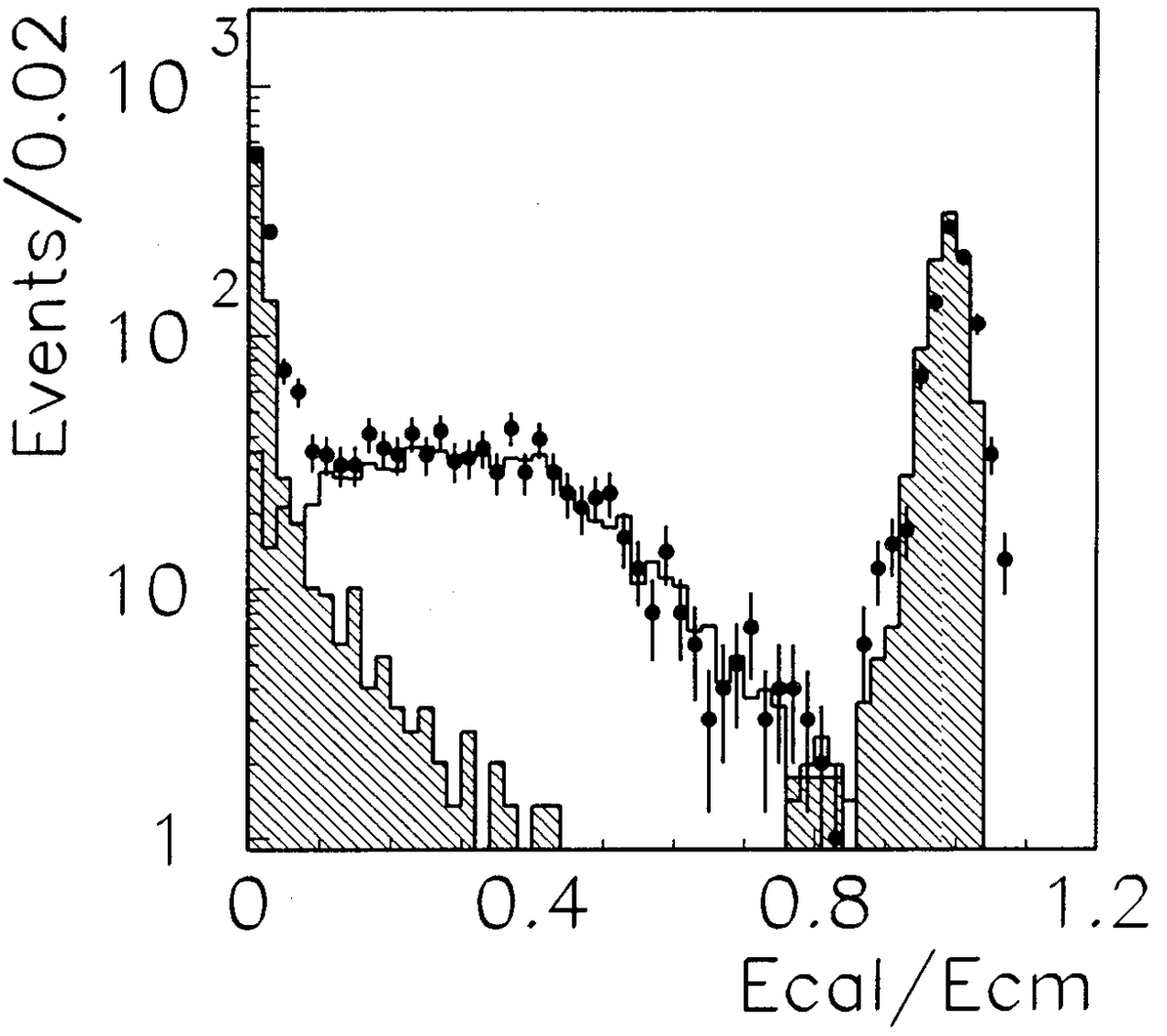

FIG. 4

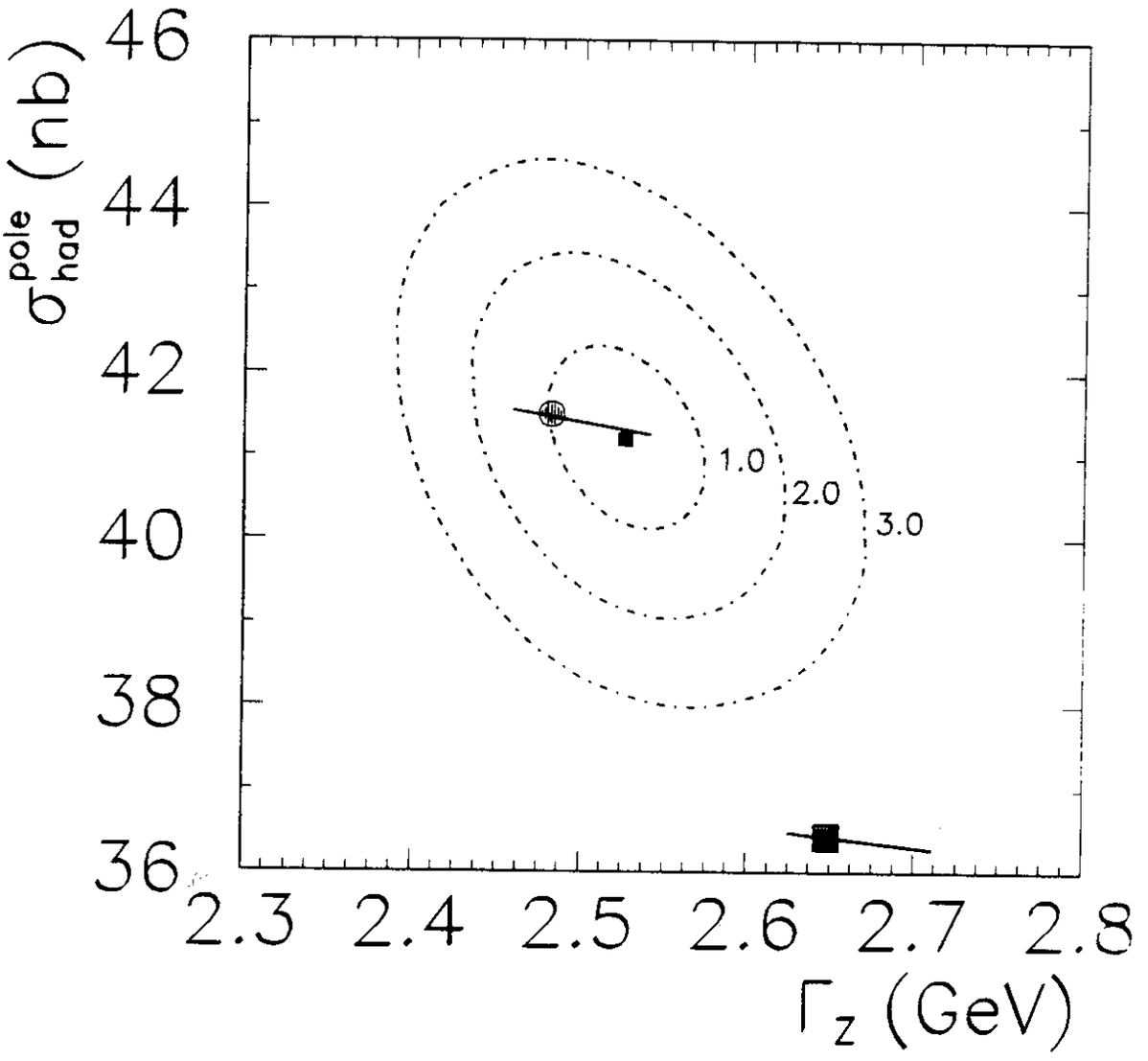
46
44
42
40
38
36
σ_{had}^{pole} (nb)
1.0
2.0
3.0
2.3
2.4
2.5
2.6
2.7
2.8
Γ_Z (GeV)

FIG. 5

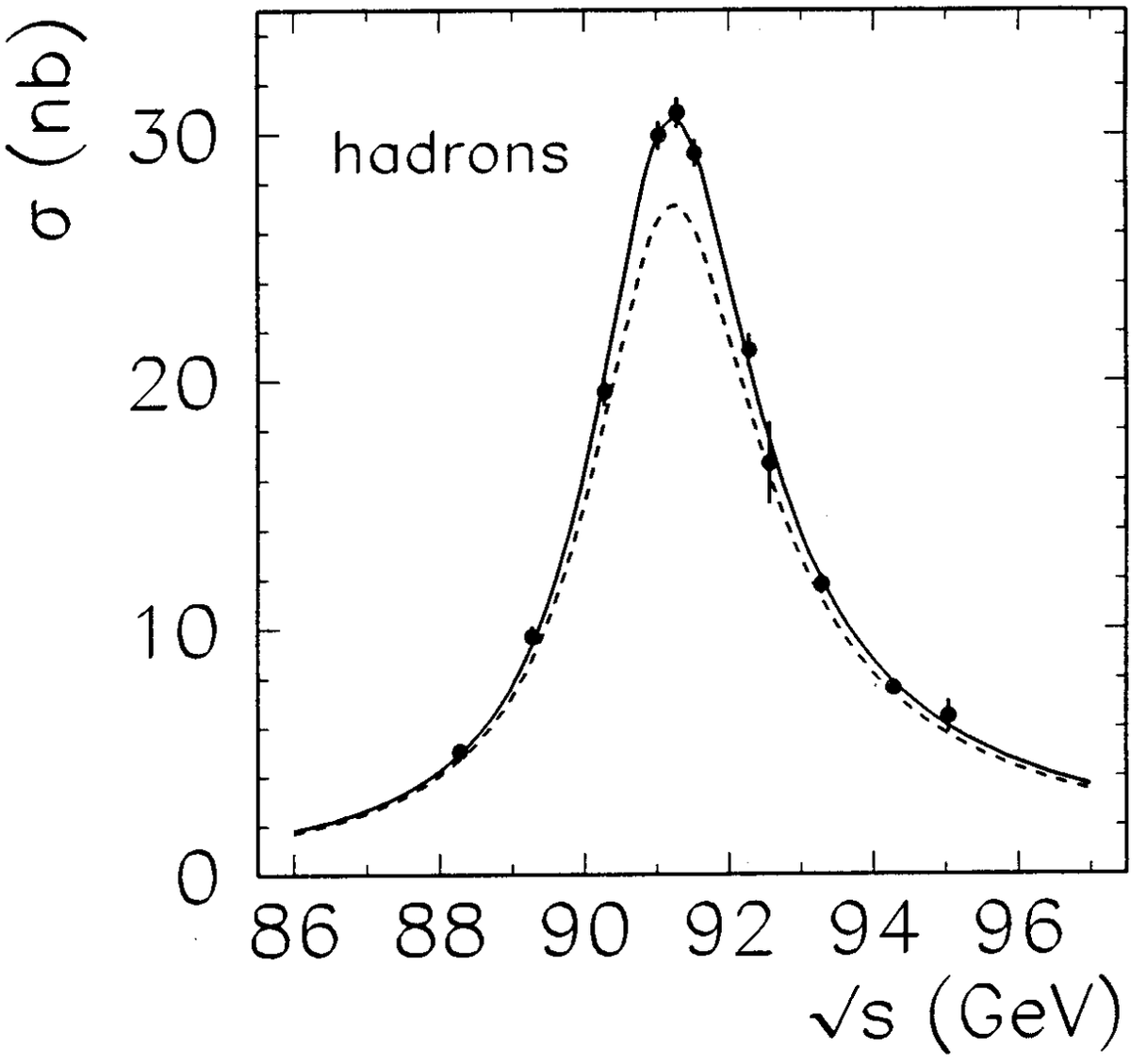

FIG. 6a

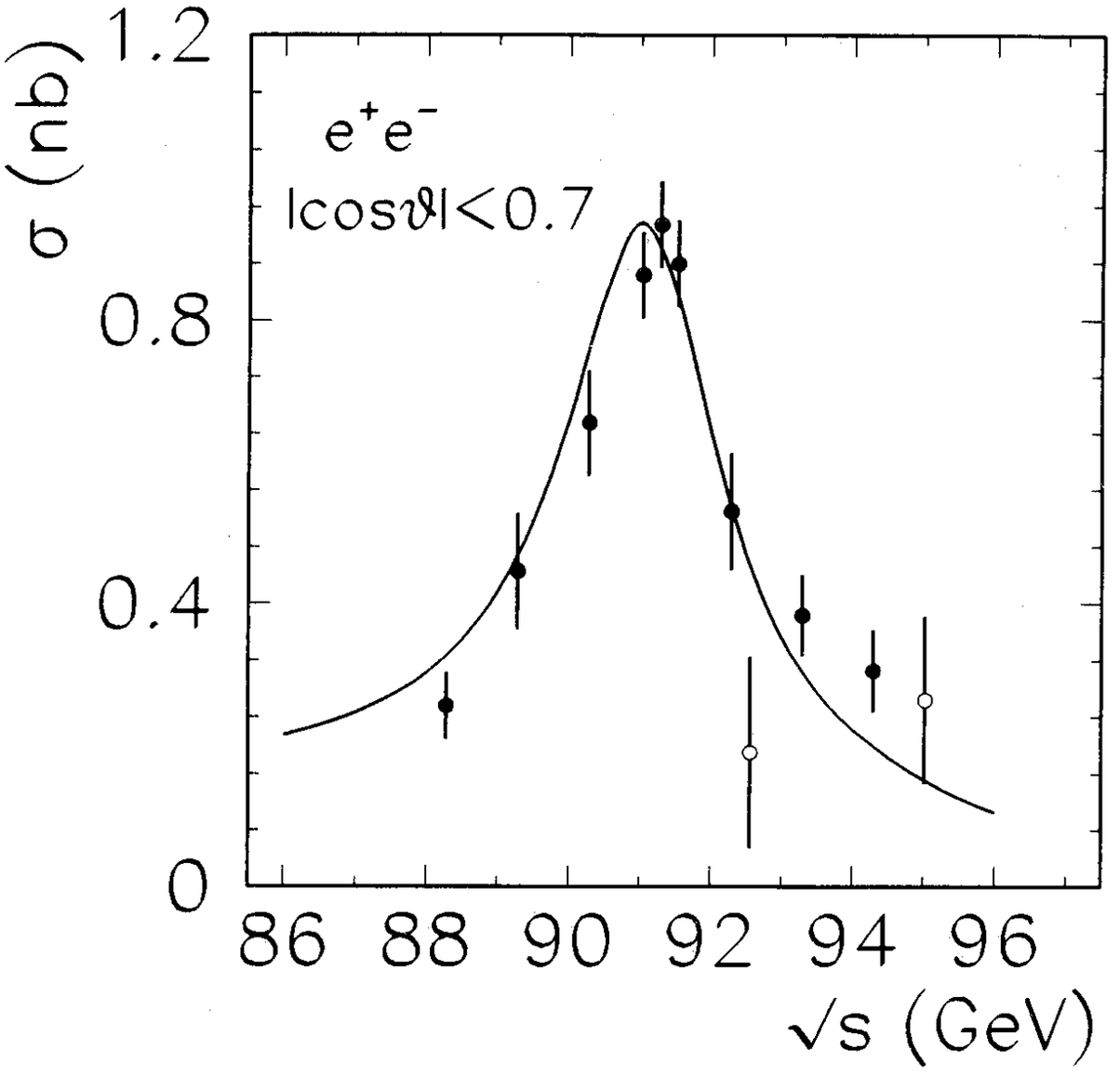

FIG. 6b

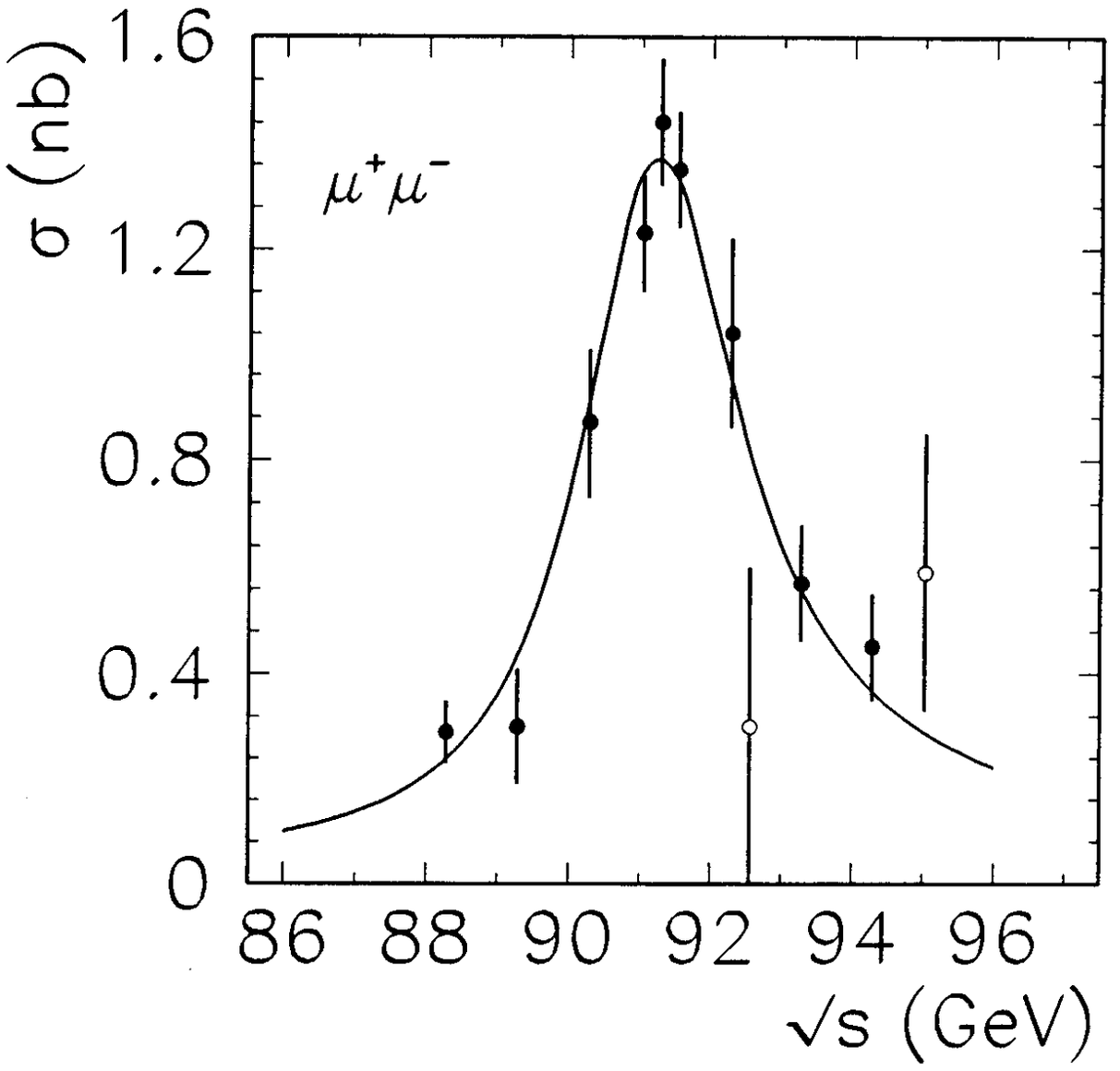

FIG. 6c

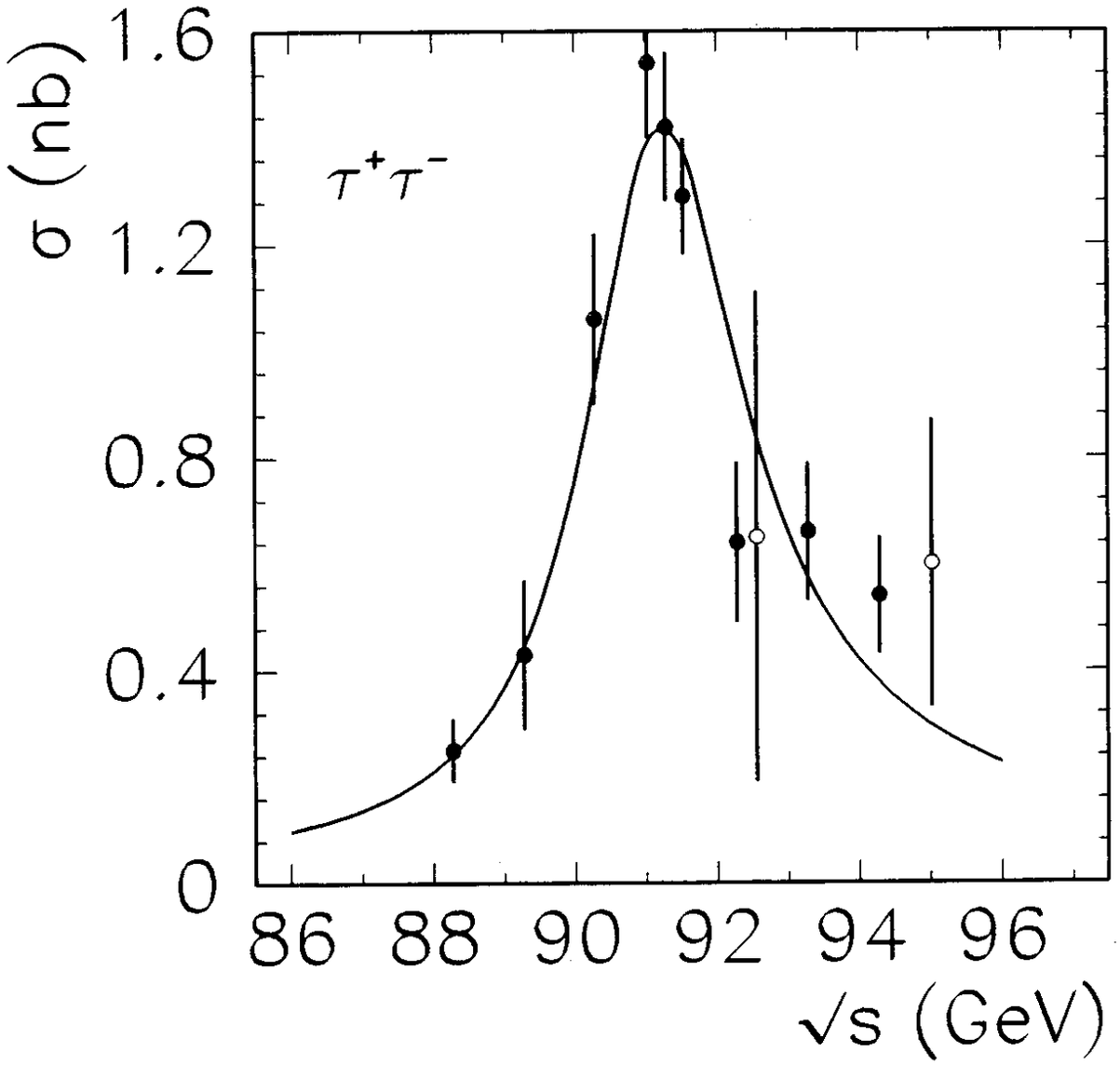

FIG. 6d

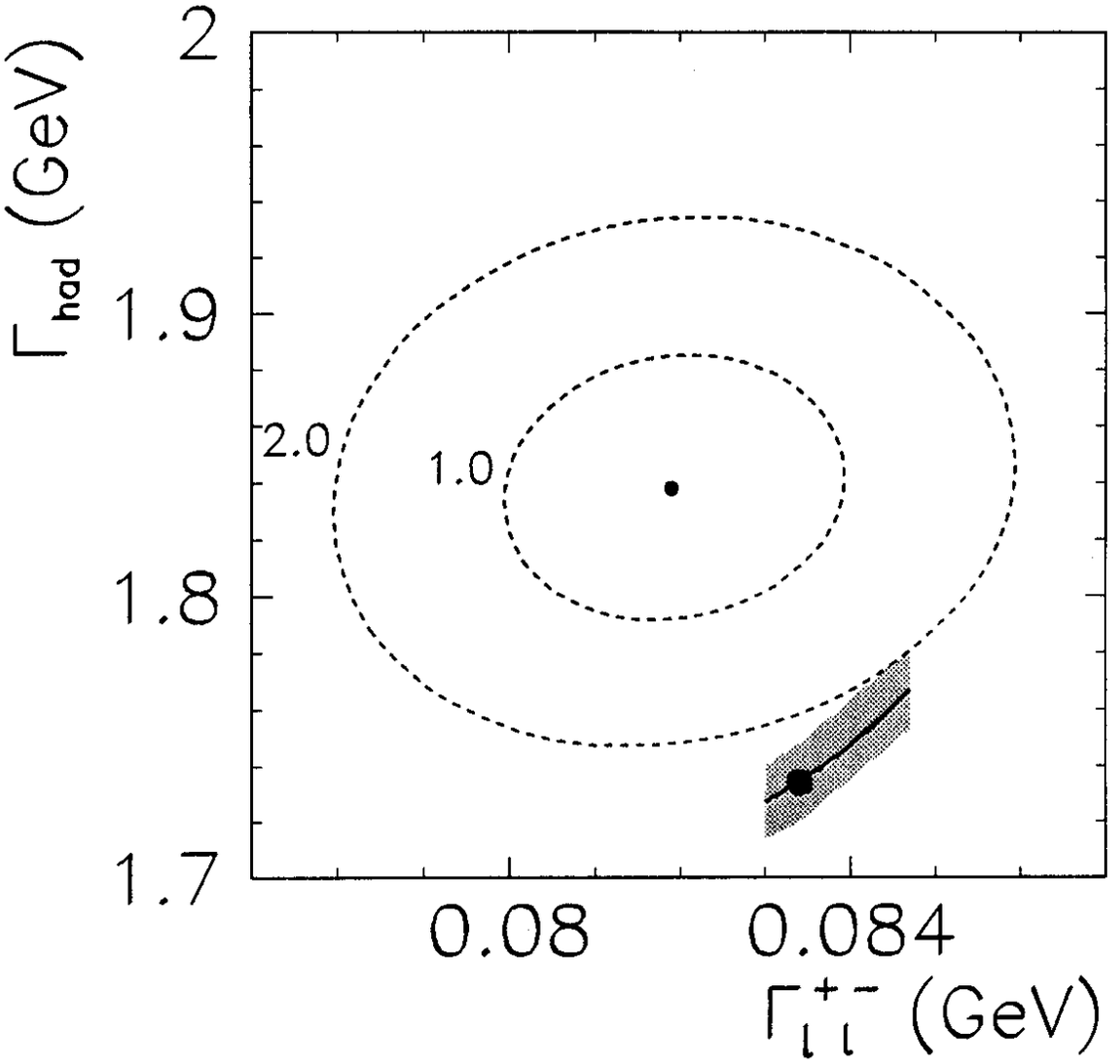

FIG. 7